Flexible Chemiresistive Nitrogen Oxides Sensors Based on a Nanocomposite of Polypyrrole- Reduced Graphene Oxide Grafted Carboxybenzene Diazonium Salts.

Djamil GUETTICHE
Ecole Militaire Polytechnique
Ahmed MEKKI (mekki_ahmedkarim@yahoo.fr)
Ecole Militaire Polytechnique https://orcid.org/0000-0002-9579-6309
BENMOULOUD Lilia
Ecole Militaire Polytechnique
Tighilt Fatma-zohra
Centre de Recherche en Technologie des Semi-conducteurs pour l'Energetique
Amar BOUDJELLAL
Ecole Militaire Polytechnique

Research Article

Keywords: NO2 sensing, chemiresistive sensor, Polypyrrole, functionalized reduce graphene oxide, 4-carboxybenzene diazonium salt

Posted Date: February 19th, 2021

DOI: https://doi.org/10.21203/rs.3.rs-218668/v1

Version of Record: A version of this preprint was published at Journal of Materials Science: Materials in Electronics on March 22nd, 2021. See the published version at https://doi.org/10.1007/s10854-021-05721-z.

Abstract

Nanocomposites of polypyrrole/reduced graphene oxide (PPy/rGO) and polypyrrole/ functionalized reduced graphene oxide with aryl 4-carboxybenzene diazonium salt (PPy/rGO-aryl-COOH) were prepared through covalent bonding by simple one-step chemical oxidative synthesis. The as-prepared nanocomposites were deposited on BOPET substrate by spin coating to test their chemiresistive sensitivity properties on a homemade modular for online detection of (NO_2) vapors at ambient temperature. Results showed that PPy/rGO-aryl-COOH forms a homogeneous nanocomposite within the size of 80 nanometers and improvement of the crystalline ordering. The more enhanced NO_2 sensing properties have been shown by PPy/rGO- aryl-COOH in terms of higher sensitivity (1.01%/ppm), the faster response time (129 s), and the detection limit of (2ppm). Reproducibility features were also investigated.

Moreover, humidity rates and temperature effects were also tested. Finally, impedance spectroscopy is conducted in the fresh air and in the presence of gas. These results highlight the paramount role of functionalization of reduced graphene oxide (rGO-aryl-COOH).

1. Introduction

As widely reported through the literature, polypyrrole/graphene nanocomposite is being used in numerous fields such as chemical sensing [1-3], biosensing [4], energy storage and energy conversion [5], electromagnetic absorption [6], and corrosion protection [7] owing to their synergetic effects resulting in improved properties. These features have brought out attention, particularly in the chemical sensing field, through preparing novel materials and sensitives elements attempting to detect nitrogen dioxides (NO_2). (NO_2) gas is known for its high toxicity to the environment when getting in contact with oxygen, water, and human health by developing susceptible respiratory infections leading to death. Rules and environmental restrictions have increased the need for its detection at low concentrations, particularly for controlling emissions from different processes [8].

Moreover, NO_2 is one of the decomposition products of nitrate ester energetic materials, causing an alteration in their physical and chemical performance properties, leading to auto-ignition under particular conditions occasioning significant damages. Therefore, rapid sensing of NO_2 at the ppm level is cruelly needed to overcome all the above-cited problems and anticipate catastrophes. The advanced of the existing sensors based on metal oxides is braked by their high functioning temperatures, reducing their lifecycle stability and making them highly power harvesting. Thus, the present work comes to place a patch in the puzzle by preparing new nanocomposite material and exploring the surface functionalization influence on the expected sensing properties toward nitrogen dioxide.

Polypyrrole (PPy) is attracting more interest from day to day in raison of its rapid and facile synthesis, by chemical, electrochemical, or irradiation techniques (UV, microwaves, and sonochemistry), its electrical conductivity, reduction-oxidation property, and good long-lifetime at room temperature [9]. Moreover, the modification of dopant nature can quickly help to tune the morphology, surface area, and electrical

properties in the desired applications [10-12], such as gas sensors, lower detection limit, rapid response time, and improved sensitivity is highly required. Although of all what has been experienced about the dopant role in the gas sensors fields [13], there are always some drawbacks that need to be improved. Thus, efforts are now oriented to combining polymers with another nanomaterial to reach more perfection by seeking the synergetic effect and new functionality raising from the two materials. Literature is full of reports, where different strategies of preparing PPy nanostructure with different metals types such as PPy-Ag [14], PPy-Pt [15], PPy-TiO_2 [16], PPy-ZnO [17], PPy/ZnO-SnO_2 [18]; PPy-NiO [19], PPy-WO_3[20], PPy-Fe_2O_3 [21], to name but few, have been reported. However, carbon-based nanomaterials, particularly graphene, have attracted much attention owing to the outstanding feature [22], and high chemical stability, making them usable as added charges to conduct sensing processes. Therefore, acceptable sensing performances have been stated when graphene-based gas sensors were used [23,24]. The synthesis of PPy-graphene nanocomposite is divided into two groups: (i) the addition of graphene into the already prepared polymer solution and (ii) in situ addition of graphene during the polymerization reaction. However, the associated problem in these cases is the agglomeration of graphene in the polymer matrix. Therefore, dispersion in organic and aqueous solutions is enhanced by their surface functionalization. Numerous approaches were recommended to tie conductive polymers and graphene. For instance, primeval or oxidized graphene [25], sulfonated graphene was directly polymerized with pyrrole. Recently, reports are portraying new methodologies using diazonium salts as a combination agent [26]. The straightforwardness of procedures has made using diazonium salts a well-dressed technique for treating various surfaces such as semi-conductor, metals, and sp^2 carbon. In addition to what aryl diazonium salts could control the interfacial properties, they will increase dispersion in solution. Thus, in the polymer matrix, they will also offer various functional groups to the host polymer to edge sensing. The main descriptions of PPy-graphene nanocomposites preparation are related to their powder form [27]. However, for emerging flexible devices, PPy-Graphene films need a direct deposition onto the flexible substrates. Due to the difficulty of handling such nanocomposite, many procedures were adopted, ranging from the in-situ deposition such as chemical and electrochemical to the ex-situ ones, such as dip coating, spin- coating and drop- coating [28]. Electrochemical techniques have a drawback, as they need electrically conductive substrates, and films obtained from chemical methods suffer from the worst homogeneity, whereas spin coating is simple process providing a deposition of homogeneous thin nanocomposite films on a large variety of insulating substrates with controlled thickness [29].

Hereby, we describe a one-stage synthesis of nanocomposite material based polypyrrole (PPy)/ reduced graphene oxide-grafted carboxybenzene-diazonium salts (PPy/rGO-aryl-COOH). Then, we report a comparison of NO_2 sensing on two types of PPy nanocomposites films chemically polymerized with only reduced graphene oxide rGO and others with functionalized reduced graphene rGO-aryl-COOH, and deposited on indium tin oxide (ITO) substrates using spin coating technique. We demonstrate that diazonium functionalized reduced graphene oxide improves the exfoliation and dispersion in the solution and provides a larger molecular function to make PPy-rGO-aryl-COOH exhibiting a larger response to NO_2 gas at room temperature (at (ppm) level). Moreover, it shows reversible behavior and stability, which might be offering it a longer working life.

2. Experimental

2.1 Ingredients

Pyrrole obtained from (Sigma-Aldrich, within a purity>98%) was refined under reduced pressure and then refrigerated at 4°C in the dark. Ammonium Peroxydisulfate and HCl were purchased from Analar Normapur within a respective purity of 98 % and 37%. Analytical grade solvents and deionized (DI) water were used throughout the preparations. Merck supplied sulfuric acid (H2SO4) (98%), Potassium permanganate (KMnO4) (98%), and phosphoric acid (H3PO4) (85%), Graphite fine powder extra pure (≥ 99.5 %, particles size < 50 µm), and hydrogen peroxide (H_2O_2) (30%) were acquired from Sigma-Aldrich. 4-Aminobenzoic acid (Reagent Plus®, ≥99 %), Isopentyl nitrite (96%) is purchased from Sigma Aldrich. The BOPET substrates (thickness, 25µm) from Sigma-Aldrich. Pieces sizes at 30 mm × 10 mm to carry out the surface washing. Sheets were cleaned using chloroform, DI water, and ethanol in the ultrasonic bath for 30 min, and then dried out at 70 °C for 4 h.

2.2 Techniques

Spin coater type Ossila is used to prepare thin film layers. FTIR spectrometer type Thermo-Scientific Nicolet 8700 used 4000-400 cm^{-1} wavenumber with a resolution of 4 cm^{-1}, over 50 scans. Raman diffusion was performed on Thermo-Scientific (RAMAN DXR2) spectrometer. X-ray diffraction (XRD) was realized using a diffractometer type X'Pert PRO (PANalytical) at 45 kV and Cu monochromatic radiation at (1.54060 A) wavelength, scanning was in the range of 5° to 90°. SEM images were captured on Microscope type (FEI-Quanta 600). Four-point probe technique type Jandel RM 3000 was used to measure films electrical conductivity.

2.3 Graphene oxide (GO) preparation

The graphene oxide (GO) was synthesized according to the improved methods described in work given in [30]. A mixture of H_2SO_4/H_3PO_4 at a ratio of (360:40 mL) was added to an already prepared solution of graphite (3.0 g, 1 wt equiv) in $KMnO_4$ (18.0 g, 6 wt equiv), generating a rise of temperature to 40 °C. The reaction was then heated to 50 °C and kept under stirring for 12 h. The reaction cooled to room temperature. Residual permanganate was reduced by adding 3 mL of 30% H_2O_2 to the suspension, and subsequently, the mixture changed its color from brown to yellow. Finally, filtration and washing were done with aqueous HCl solution (1:10: HCl: H_2O) and then distilled water. The resulting solid was dried under air for 20 h to obtain GO.

2.4 Preparation of reduced graphene (rGO)

100 mg of GO was mixed with (100 mL), and then sonicated. The solution was mixed with hydrazine hydrate (1.00 mL, 32.1 mmol) and then refluxed for 24 h until rGO start to precipitate out. The obtained product was filtrated, washed with water (5X) and methanol (5X), and then dried [31].

2.5 In-situ functionalization of reduced graphene oxide with aryl 4-carboxybenzene diazonium salt (rGO-aryl-COOH)

The occurrence of Diazonium functionalization was according to the literature's method and our earlier works [32,33]. An aqueous solution of 1 g of synthesized GO in 250 mL of de-ionized water, was sonicated for 30 min, then 5 mL of 50% hydrazine hydrate was dropped. Later, the mixture was subjected to stirring for 4 hours at 100 °C. Diazonium salts was in-situ grafted on the rGO, where 4 g of 4-aminobenzoic acid and 3 mL of isopentyl nitrite were vigorously mixed at 80 °C overnight. The obtained product was filtered and washed with water, followed by dimethylformamide. The black solid eventually dried under high vacuum conditions.

2.6 Synthesis of Polypyrrole/rGO-aryl-COOH nanocomposites

Figure 1 shows the different steps of polypyrrole/rGO-aryl-COOH nanocomposites preparation. Dispersion of 4 mg of rGO-aryl-COOH in 50 mL of methanol was assisted by ultrasonication for 30 min. Then, 2.23 M of pyrrole was dropped into the solution under continuous ultrasonication for 30 min. While the temperature was maintained close to the range of 0 °C to 5°C, the quantity of 2.5 M of $FeCl_3$ was progressively introduced to the mixture of pyrrole and rGO-aryl-COOH then kept under forceful stirring for 6 h. PPy can be grown on the surface of functionalized reduced graphene oxide due to the susceptible hydrogen bonding raising between the carboxybenzene functionalized reduced graphene oxide and polypyrrole. Finally, the obtained nanocomposite was filtered, washed, then dried in a vacuum. The same steps were followed for the preparation of both of PPy/rGO nanocomposite.

2.7 Nanocomposites thin films preparation for sensing tests

After the dispersion of 0.1 g of each PPy nanocomposite with rGO and rGO-aryl-COOH in acetone under the effect of ultrasonic waves for 30 min, they were then dropped on BOPET to be spin-coated at 1000 rpm for 60 s. Finally, residual acetone was evaporated at 40 °C. As shown in fig.2, obtained films were of homogeneous continuous coating and thickness of 10±1 µm.

2.7 Chemiresistive sensor system set up

Homemade platform was used to carry out the sensing tests. A legend in Fig. 4 depicts all the related details. Flexible polymer nano-composite placed on mobile piston through a polyethylene tube possessing an inner volume of 60 mL. Set on the top of the tube, a Four-point probe connected to device type Jandel RM3000 for online electrical conductivity measurement. Samples are inserted through a small puncture using a microliter syringe (contact point). We produced the environmental humidity by simple evaporation of distilled water directly connected to the test compartment. The experiments were conducted at temperatures around 25 ^{O}C. The exact concentrations of emitted vapors were calculated according to an equation in our previous works on VOC and ammonia sensing [15]. The percent response was determined from the response curves according to the following relations:

$$S = \frac{|R_g - R_a|}{R_a} * 100\% \quad (1)$$

When R_g is the response value of sensor thin layers under measuring gas, and R_a is the response value of fresh air.

3. Results And Discussion

3.1 FTIR characterization

Figure 5 displays the FTIR spectra of the prepared graphene samples GO, rGO and rGO-aryl-COOH, and their nanocomposites. According to Fig. 5a, for the GO, broadband appeared at the wavenumber of approximately 3428 cm^{-1} characteristics of the OH elongation vibration of the -COOH groups and water molecules interspersed. Also, the elongation C = O was seen at 1720 cm^{-1}, while the stretch of epoxy group C-O-C can be observed at a wavenumber of 1298 cm^{-1} and at 1008 cm^{-1} [34]; the peaks at 1069 and 1170 cm^{-1} are attributed to the C-O bond of the alkoxyl and carboxyl groups, respectively. The peak found at 885 cm^{-1} has been ascribed to aromatic C-H bonds of pyrrole [34]. In all of these groups, it has been confirmed that oxygen molecules strongly occupy the edges and surfaces of GO. It can be concluded that GO has been successfully synthesized.

In Fig. 5b, the peak at 3439 cm^{-1} has become narrower compared to that of rGO, showing that the hydroxyl and carboxyl group have been eliminated significantly. We noted the intensity reduction of the other peaks at 1720, 1298, 1008, 1069 and 885 cm^{-1}. Therefore, peaks at 1637, 1444 and 1119 cm^{-1}, can be affected by the extending vibration of the C = C bond, the C-OH strain vibration, and the C-O elongation of the alcohol group, respectively [34]. Consequently, the oxygen-containing functional groups have been partially eliminated from the rGO with success, and small functional group residues have still persisted at the peripheral and basal plane of rGO.

The FTIR spectrum of rGO-aryl-COOH presented in Fig. 5c**,** shows: a wide and intense band at 3422 cm^{-1}, which is distinctive of the COOH groups elongating vibration, a peak at 1723 cm^{-1} attributed to C=O stretching of the –COOH group and a peak at 1561 cm^{-1} corresponds to the vibrations of the C = C bonds. This indicates the presence of an Aryl-COOH group. The peaks at 2926 and 2856 cm^{-1} have been attributed to the C-H stretching vibration of the sp^3 carbon, which proves that the Aryl-COOH functional groups had been effectively grafted on top of the surface of rGO.

The assessment of Fig.5b related to PPy / rGO composite shows the presence of polypyrrole characteristic peaks at 1551 and 1315 cm^{-1} (the elongation C-C and C-N of the pyrrole ring). The peak at 1040 cm^{-1} corresponds to the C-H vibrations of the ring pyrrole in the plane. The peaks at 923 and 1180 cm^{-1} are allotted to the bipolar state of PPy [35]. The peaks corresponding to the C-H strain vibration of the polymer ring off-plan are observed at around 781 cm^{-1} [36].

Spectra Fig. 5c, of PPy/ rGO-aryl-COOH shows the presence of peaks due to oxygen functional groups, in addition to the characteristic peaks of PPy, at 1494, 1367,1206 and 929 cm^{-1}, which can be attributed to the C-C and C-N elongation of the pyrrole ring and the bipolar state of PPy, respectively [35]. The wideband at 3469 cm^{-1} can be assigned to the amine groups of the polypyrrole and O-H groups in rGO-aryl-COOH. The peaks at 1741 and 1600 cm^{-1} are attributed to carbonyl groups and the bond C = C, respectively, which confirms the polymerization of PPy and the composite formation [37].

3.2 Raman characterization

Figure 6 illustrates Raman spectra, GO, rGO and rGO-aryl-COOH, and Table 1 lists the characteristics of the latter. Raman spectroscopy is very useful for observing structural changes in the samples through oxidation, exfoliation, reduction, and functionalization. The D band and the G band, characteristic of graphene have been demonstrated. Generally, the G band corresponds to the bonds of the sp^2 carbons in a conjugated carbon network [38]. The D band (or diamond band) is only observed in defects corresponding to the signal of the sp3 carbons present in a carbon crystal such as a diamond. It is observed only in defective graphene [39]. Defects density can be estimated by measuring the ratio between intensity (I_D/I_G) of the D band and the G band [38,39].

A sharp and intense G band at 1568 cm^{-1} and a feeble D band at 1345 cm^{-1} can be found in the graphite sample with a low I_D / I_G value of 0.31, indicating the presence of the sp^2 hybrid carbon atoms with a minimal number of defects [38]. Another single peak perceptible at 2700 cm^{-1}, indicating the stacking of graphitic multilayers [39].

When oxidizing the graphite, the GO sample shows an intense D band at 1364 cm^{-1}, while the G band widened and moved to an upper wavenumber at 1614 cm^{-1}, caused by the presence of isolated double bonds, which demonstrates the introduction of defects in the structure of graphene by the incorporation of oxygen groups [7]; therefore, the corresponding ratio I_D / I_G augmented to 1.02. A smaller defect density with an I_D / I_G ratio of 1.00 was observed after hydrazine reduction in rGO spectra. The G band has also shifted to an inferior wavenumber (1574 cm^{-1}), signifying the regaining of the sp^2 domain of graphene to some extent by removing oxidizing groups [40].

After rGO functionalization, an increase of I_D/I_G ratio around 1.02 was observed, attributed to the aryl functions grafting. The G band has shifted slightly to a lower wavenumber p 1573cm^{-1}, which signifies the increase in the sp^2 domain and which may be due to the benzene rings of the Aryl group.

On the other hand, the 2D band consists of two peaks named 2D and D + D ', as observed in the Raman spectra of the samples GO and rGO and rGO-aryl-COOH, which indicates a decrease in the number of layers of graphene in these samples compared to the graphite sample [39].

The superposition of the Raman spectra of the composites PPy / GO, PPy / rGO and PPy / rGO-aryl-COOH with their charges is illustrated in Fig.7 the corresponding values are precised in Table 2.

There are two peaks around the D band and the G band within all samples, the relatively large shape suggests a partially disordered structure demonstrating short conjugation sequences. There is also a decrease in the composites I_D / I_G ratios compared to their pure fillers, indicating the increase in the sp^2 domain, which may be due to incorporating polypyrrole into the material. Compared to the starting charges, the D and G bands have changed to lower wavenumbers, demonstrating that the conductive polymers do interact with the charge [41].

The PPy / GO spectrum can be seen as an appearance of low-intensity peaks at 615 cm^{-1} (torsion ring), at 940 and 992 cm-1, which matches the polaronic and bipolaronic quinoid structure, respectively. Regarding the rGO / PPy spectrum, two more peaks are observed at 968 and 1042 cm^{-1}, which correspond to the deformation of the bipolar [12].

The Raman spectra of the nanocomposites PPy/ rGO-aryl-COOH shows four new peaks from the PPy can be indexed at 930, 959, 1057 and 1244 cm^{-1}, except the D and G bands of the rGO-aryl-COOH sheets, which correspond to the polaronic structure, bipolaronic quinoid, symmetric and antisymmetric CH bending vibration in the polaron plane, respectively [12]. Leading to high conductivity [10].

3.3 X-ray diffraction Characterization

Aiming to get more insight, a comparison between X-ray diffraction patterns of GO, rGO, and rGO-aryl-COOH is shown in Fig. 8. The graphite showed a sharp, high intensity diffraction peak, at a value of 2θ of about 26.41°, with a parameter hkl (002). This result confirms the arranged layer structure with an inter distance (d_{002}) of 0.334 nm along with the (002) orientation and which is consistent with the reported literature [42].

The DRX profile of the GO shows a new peak at 2θ = 9.4°, with a parameter hkl (002). It arises from the presence of both of sp^2 domains of graphene and oxidized sp^3 domains [43]. As a result, the interlayer distance increased (d_{002}=0,92 nm). This has been accredited to the spacing induced by the presence of functional oxygen groups and water molecules in the interlayer space of GO [43].

After the chemical reduction of GO, a wider peak is observed for rGO at 2θ = 26.19 °, thus a significant decrease (or disappearance) of the peak at 2θ = 9.4 °. This points out that the π-conjugated structure of graphene has been significantly reinstated [42]. Also, the d_{002} spacing of rGO was reduced to 0.34 nm, demonstrating the removal of the functional groups containing oxygen.

The broad peak at 2θ = 26.19 ° for rGO implies the random arrangement of the crystal phase (002) for the high crystallization structure of graphite [60]. In the rGO-aryl-COOH diffractogram, we notice the appearance of new peaks, very sharp at the different Bragg angles (2θ = {16.67 °; 17.41 °; 18.47 °; 25.08 °; 26, 31 °; 29.26 °}), which can probably be linked to the crystallization of the Aryl functions. This is possibly due to the self-organization of the aryl groups and grafting of the latter at well-determined positions in the rGO plan [44].

PPy/ rGO composite presented on Figure 9 shows a wide halo at 2θ = 26.14 °, typical of PPy, indicating the presence of an amorphous part in the composite [5]. In contrast, the original diffraction peak of rGO disappeared. Indicating the exfoliation of rGO and the PPy chain are formed on the rGO surface during the polymerization reaction [3].

The PPy/ rGO-aryl-COOH composite in Fig. 9 had a wide peak at 25 °, representing the existence of PPy. In addition, the characteristic peaks of rGO-aryl-COOH disappeared in the PPy /rGO-aryl-COOH composite, indicating that rGO-aryl-COOH showed no accumulation and was used entirely as a substrate for PPy [3].

3.4 SEM Characterization

Figure 10a, shows the micrograph of reduced graphene oxide (rGO). The surface contained thin crumpled leaves, which are settled randomly, tightly associated with each other to form a disordered structural material [45]. The Van der Waals interaction between graphene layers leads to a significant agglomeration due to being highly hydrophobic.

The SEM on Figure 10b, of the functionalized reduced graphene oxide rGO-aryl-COOH, presents a morphology of crumpled thin sheets, which gives it a large surface area. It can also be observed that the shape of the peripheral contour of carboxybenzene-functionalized graphene is tilted because of the carboxyl group effect.

Figure 10c shows the formation of highly agglomerated PPy/rGO nanocomposite, probably caused by the strength of the hydrogen bond and the π-π interaction between pyrrole and rGO [46]. In contrast, Figure 10d shows the of PPy/rGO-aryl-COOH nanocomposite. PPy has a wrinkled shape forming a mesh structure, grown on the surface of functionalized reduced graphene oxide nanosheets, indicating that the PPy network is firmly joined with the graphene nanosheets. These morphological features are likely to play a considerable role in NO_2 absorption because it provides a large adsorption surface and facilitates the adsorption of NO_2.

3.5Conductivity measurements

Table 3 gives the room temperature electrical conductivity values of (σ) PPy/rGO and PPy/ rGO-aryl-COOH nanocomposite, where the film (PPy/ rGO-aryl-COOH) shows the higher values. These propose that the PPy developed on the carboxyl-benzene functionalized graphene has a better chain arrangement, increasing the PPy/ rGO-aryl-COOH conductivity. This could be related to the electron-withdrawing groups rising from carboxyl-benzene functionalization, thus expanding the electron transfer density between the graphene plane and the carboxyl group. This increase in density leads to a rise in conductivity [47]. The variation of conductivity can be regarded from SEM results and X-ray diffraction obtained earlier in figures 8, 9 and 10, where the crystallinity of PPy chain structure conferred by grafted presence rGO-aryl-COOH sheets as well as they help the inter-chain hopping of charge carriers.

3.6 Chemiresistive gas sensing characteristics

On Figure 11, we investigate the comparison of the sensing selectivity of nano-composite PPy/rGO and PPy/ rGO-aryl-COOH toward the same concentration of different gases NO_2, NH_3, H_2S and SO_2. PPy/rGO-aryl-COOH thin film has shown big selectivity to 20 ppm of NO_2 over the former gases. The high selectivity of PPy/rGO-aryl-COOH establishes a suitable material for detecting NO_2 gas at low concentration. This selectivity improvement is credited to the synergistic effect of rGO-aryl-COOH and PPy.

3.6.1 Response time

As shown in Figure 12, the response time was observed very fast, around 129s and 199s for the nanocomposites PPy/ rGO-aryl-COOH and PPy/rGO, respectively. However, after removing the external excitation, the recovery time was found around 114 s and 145 s for the nanocomposites PPy/ rGO-aryl-COOH and PPy/rGO, respectively. This emphasizes the effect of the surface functionalization on the performances of the principal sensor.

3.6.2 Static study

Repeatability of the PPy/rGO and PPy/ rGO-aryl-COOH based gas sensor is given in Fig. 13; five rounds of responses to NO_2 have been completed within the exposition of the nanocomposites to 2 ppm. An excellent repeatable and stable behavior is observed after cycles for gas sensing. Nitrogen dioxide a strong oxidant, PPy/rGO-aryl-COOH and PPy/rGO exhibit preferentially the p-type behavior, causing a proliferation of charge carriers number decrease in the nanocomposites resistances. The composite PPy/rGO-aryl-COOH showed a high response to PPy/rGO due to the diazonium functionalization of the withdrawing groups. Furthermore, the charge transfer between PPy and rGO-aryl-COOH can be more efficient due to the interfacial affinity provided by the interaction of carboxyl groups and non-binding nitrogen atom doublet of polypyrrole. Also, the carboxyl groups can probably participate in the sensor response by favoring NO_2 adsorption.

3.6.3 Dynamic study

NO_2 concentrations ranging in the 1-20 ppm were injected as illustrated on Fig. 14. Change in the curve response amplitude was observed proportionally when increasing NO_2 concentration. The amplitude is more intense, notably PPy/rGO-aryl-COOH. This put forward role of functionalization in improving the sensor response. During the recovery process, both of the tested films rapidly regain the baseline, signing their reversibility. The PPy/ rGO-aryl-COOH nanocomposite shows encouraging prospects as a potential material for NO2 detection in atmospheric conditions in terms of comparison between the two-tested nano-composites.

3.6.4 Sensors response under temperature variation

As the PPy/ rGO-aryl-COOH has shown high response performances, the following sections are dedicated only to the behavior study of PPy/ rGO-aryl-COOH. Aiming to follow temperature influences, PPy/ rGO-

aryl-COOH was heated into different temperatures and values until 80°C. The corresponding responses are presented in Fig. 15 and deduced sensitivity values are given in Table 4 below. Although the applied temperature environment has a total of sensitivity reduction around 20%, such comportment could reduce site activity in the composite layer and hamper the interactions development. However, we can observe that temperature doesn't affect the sensitivity significantly in an immense magnitude, confirming that PPy/ rGO-aryl-COOH preserve its performances even under a variable temperature environment

3.6.5 Influence of relative humidity

Injection of 2-ppm concentration of NO_2 gas was carried out under a humid atmosphere. A hygrometer (Omega type HH314A) was used to indicate The relative humidity (RH) generated by injecting water vapor in the test chamber at rates ranging from 20% to 80%, as illustrated in Fig. 4. The inverse proportionality of the sensor response with humidity shown in Fig. 16, demonstrates a diminution more than 50%, establishing the substantial humidity impact on sensor efficiency. This result may be due to inhibition of the active site by a hydroxyl group, when they are bridged with carboxylic entities through a hydrogen bond.

3.6.6 Impedance spectroscopy study

Impedance spectroscopy is used to characterize contributions arising from the interactions of different components of PPy/ rGO-aryl-COOH and PPy/rGO film with the gas. Two environments were used to conduct the impedance measurements (pure air and NO_2 at a concentration of 20 ppm). Figure 17 shows the plot obtained spectra in the form of Nyquist. Resulted impedance spectra are plotted from low frequency to high frequency region in the form of a semi-circle, the obtained values can be set into an equivalent circuit as presented in Fig. 18, consisting of free frequency resistance (R_0), resistance (R_1) and capacitor (C_1) in parallel. Figure 17, shows the identification between experimental data and fitted curve. Table 5 presents the physical measurements before and after exposure to NO_2 gas. It was found that R_0 is the same in gas and air conditions. However, R_1, R_2 and C_1 do not alter dramatically when exposed to the NO_2 gas. This finding is supported by the fact that upon interaction of NO_2 with PPy, charge carriers are produced at the surface of PPy, lowering the inter-grains resistance, on the one hand, facilitating charge transfer between PPy and rGO, and thus increasing the inter-grains capacitance, on the other hand.

Table 6 presents a comparison of chemiresistive sensors performances according to the materials nature based as the sensing interfaces.

Conclusions

A flexible nanocomposite of polypyrrole with graphene functionalized surface film destined as dioxide nitrogen sensor has been elaborated following in situ one-step polymerization of pyrrole at room temperature. Surface functionalization of reduced graphene oxide by diazonium salts type carboxy-

benzene has enhanced its crystallinity and, thus, nanocomposite, further improved electric conductivity. After investigations with various gases, observations have put forward the aptitude of detection selectivity toward nitrogen dioxide gas above the other vapors. The PPy/ rGO-aryl-COOH film displays good features notably (response time within few minutes, and sensitivity in (1-20 ppm) range exposure comparatively to nanocomposite film prepared only with reduced graphene, highlighting the paramount impact of surface functionalization rising from the presence of carboxylic groups which has proven its ability and capability to develop bonds with nitrogen dioxide, and influence furtherly the whole sensitivity. Moreover this founds come to confirm what was reported in the literature about the contribution of such function groups in regulating the sensor performances. The sensitivity of PPy/ rGO-aryl-COOH remains considerable under varied temperature, indicating its function ability under harsh environment film. Moreover, even with the different rates of applied humidity, the film has kept an acceptable sensitivity. Hence, PPy/rGO-aryl-COOH can be classified as one of the promising sensitive materials for dioxide nitrogen gas detection.

Declarations

Acknowledgments

Ecole Militaire Polytechnique financially hosted this work through the providing of a Ph.D. scholarship project N° 2/17/DRFPG/CMDT for GUETTICHE Djamil. The authors are also grateful to the DGRSDT/MESRS for providing assistance to this work.

Ethical procedures

The paper is submitted with complete responsibility, respecting the ethical procedure; where all concerns related to animal or human experimentation are totally discarded. Moreover, all kind of duplication, fraud or plagiarism have been correctly checked and refined.

A disclosure / conflict of interest statement

None of the authors of this paper has a financial or personal relationship with other people or organizations that could inappropriately influence or bias the content of the paper. It is to specifically state "No Competing interests are at stake and there is No Conflict of Interest" with other people or organizations that could inappropriately influence or bias the content of the paper.

References

[1] Parthasarathy Srinivasan, Madeshwari Ezhilan, Arockia Jayalatha Kulandaisamy, K. Jayanth Babu, John Bosco Balaguru Rayappan, Room temperature chemiresistive gas sensors: challenges and strategies—a mini review. J Mater Sci: Mater Electron **30**, 15825–15847 (2019)

[2] S. R. Nalage, M. A. Chougule, Shashvati Sen, V. B. Patil, Novel method for fabrication of NiO sensor for NO_2 monitoring. J Mater Sci: Mater Electron **24**, 368–375

[3] W.-K. Jang, J. Yun, H.-I. Kim, Y. S. Lee, Improvement of ammonia sensing properties of polypyrrole by nanocomposite with graphitic materials. Colloid Polym. Sci. **291**, 1095-1103 (2013)

[4] C. Ott and al, Functionalized polypyrrole/sulfonated graphene nanocomposites: Improved biosensing platforms through aryl diazonium electrochemistry. Synth. Met. **235**, 20-28 (2018)

[5] Abu Jahid Akhtar, Shubhankar Mishra, Sudip Kumar Saha, Charge transport mechanism in reduced graphene oxide/polypyrrole based ultrahigh energy density supercapacitor. J Mater Sci: Mater Electron **31**, 11637–11645 (2020)

[6] F. Wu, A. Xie, M. Sun, Y. Wang, M. Wang, Reduced graphene oxide (RGO) modified sponge like polypyrrole (PPy) aerogel for excellent electromagnetic absorption. J. Mater. Chem. A. **3**, 14358-14369 (2015)

[7] M. Marimuthu and al, Sodium functionalized graphene oxide coated titanium plates for improved corrosion resistance and cell viability. Appl. Surf. Sci. **293**, 124-131 (2014)

[8] T. Boningari, P. G. Smirniotis, Impact of nitrogen oxides on the environment and human health: Mn-based materials for the NO_x abatement. Curr. Opin. Chem. Eng. **13**, 133-141 (2016)

[9] M. Das, S. Roy, Polypyrrole and associated hybrid nanocomposites as chemiresistive gas sensors: A comprehensive review. Mater. Sci. Semicond. Process. **121**, 105332 (2021)

[10] A. T. Mane, S. D. Sartale, V. B. Patil, Dodecyl benzene sulfonic acid (DBSA) doped polypyrrole (PPy) films: synthesis, structural, morphological, gas sensing and impedance study. J Mater Sci: Mater Electron **26**, 8497–8506 (2015)

[11] S. Geetha, D. C. Trivedi, Synthesis, characterization and temperature studies on the conductivity of AlCl−4 ion doped polypyrrole. J Mater Sci: Mater Electron **16**, 329–333 (2005)

[12] Shruti Peshoria, Anudeep Kumar Narula, Study and explanation about the morphological, electrochemical and structural properties of differently synthesized polypyrrole. J Mater Sci: Mater Electron. **28**, 18348–18356 (2017)

[13] F. Merdj, A. Mekki, D. Guettiche, B. Mettai, Z. B. D. Sayah, Z. Safidine, A. Abdi, R. Mahmoud, Macromol. Res. (2018) https://doi.org/10.1007/s13233-018-6069-1

[14] J. Zhang, X. Liu, S. Wu, H. Xu, B. Cao, One-pot Fabrication of Uniform Polypyrrole/Au Nanocomposites and Investigation for Gas Sensing. Sens. Actuators B **186**, 695-700 (2013)

[15] Namrata Gaikwad, Sreenu Bhanoth, Priyesh. More, G. H. Jainb and P. K. Khanna, Chemically designed Pt/PPy nano-composite for effective LPG gas sensor. J. Nanosci. **6**, 2746-2751 (2014)

[16] M. Kumaresan, M. Venkatachalam, M. Saroja, P. Gowthaman, Significant enhancement in the hydrogen-sensing performance of polypyrrole/titanium oxide (PPy/TiO_2) hybrid sensors by a chemical oxidation polymerization approach. J Mater Sci: Mater Electron **31**, 8183–8193 (2020)

[17] H. Albaris,G. Karuppasamy, CuO–ZnO p–n junction enhanced oxygen sensing property of polypyrrole nanocomposite at room temperature. J Mater Sci: Mater Electron **30**, 9989–9998 (2019)

[18] H. A. Khorami, A. Eghbali, M. Keyanpour-Rad, M. R. Vaezi, M. Kazemzad, Ammonia sensing properties of (SnO2–ZnO)/polypyrrole coaxial nanocables. J. Mater. Sci. **49**, 685–690 (2014)

[19] S.R. Nalage, S.T. Navalea, R.S. Manec, Mu. Naushad, F.J. Stadlarb, V.B. Patila, Preparation of camphor-sulfonic acid doped PPy–NiO hybrid nanocomposite for detection of toxic nitrogen dioxide. Synth. Met. **209**, 426-433 (2015)

[20] A.T. Mane, S.T. Navale, V.B. Patil, Room temperature NO_2 gas sensing properties of DBSA doped PPy–WO3 hybrid nanocomposite sensor. Org. Electron. 19, 15-25 (2015)

[21] S.T. Navale, G.D. Khuspe, M.A. Chougule, V.B. Patiln, Room temperature NO2 gas sensor based on PPy/α-Fe2O3 hybrid nanocomposites. Ceram. Int. **40**, 8013-8020 (2014)

[22] A. K. Geim, K. S. Novoselov, The rise of graphene. Nanosci. Technol.: Int. J. (2009) https://doi.org/10.1142/9789814287005_0002

[23] GRavi Kumar, Anil Kumar, Rakesh Singh, Rajesh Kashyap, Dinesh Kumar, Rajesh Goel, Mukesh Kumar. J Mater Sci: Mater Electron (2021). https://doi.org/10.1007/s10854-020-04940-0

[24] S. Basu et P. Bhattacharyya, Recent developments on graphene and graphene oxide based solid state gas sensors. Sens. Actuators B **173**, 1-21 (2012)

[25] H. Bai, K. Sheng, P. Zhang, C. Li and G. Shi, Graphene oxide/conducting polymer composite hydrogels. J. Mater. Chem. **21**, 18653 (2011)

[26] C. Cao, Y. Zhang, C. Jiang, M. Qi, and G. Liu, Advances on Aryldiazonium Salt Chemistry Based Interfacial Fabrication for Sensing Applications. ACS Appl. Mater and Interfaces. **9**, 5031-5049 (2017)

[27] S. Bose, T. Kuila, M. E. Uddin, N. H. Kim, A. K.T. Lau, J. H. Lee, In-situ synthesis and characterization of electrically conductive polypyrrole/graphene nanocomposites. Polymer. **51**, 5921-5928 (2010)

[28] Metin Yurddaskal, Mustafa Erol, Erdal Celik, Carbon black and graphite filled conducting nanocomposite films for temperature sensor applications. J Mater Sci: Mater Electron. **28**, 9514–9518 (2017)

[29] S.T. Navale, A. T. Mane, M. A. Chougule, R. D. Sakhare, S.R. Nalage, V.B. Patil, Highly selective and sensitive room temperature NO_2 gas sensor based on polypyrrole thin films. Synth. Met. **189**, 94-99 (2014)

[30] D. C. Marcano, D. V. Kosynkin, J. M. Berlin, A. Sinitskii, Z. Sun, A. Slesarev, Lawrence B. Alemany, Wei Lu, J. M. Tour, Improved Synthesis of Graphene Oxide. ASC Nano. **4** ,4806-4814 (2010)

[31] S. Stankovich, D. A. Dikin, R. Piner, K. A. Kohlhaas, A. Kleinhammes, Y. Jia, Y. Wu, S. B. T. Nguyen, R. S. Ruof, Synthesis of graphene-based nanosheets via chemical reduction of exfoliated graphite oxide. Carbon. **45**, 1558–1565 (2007)

[32] A. A. Mohamed, Z. Salmi, S. A. Dahoumane, A. Mekki, B. Carbonnier, M. Chehim, Functionalization of nanomaterials with aryldiazonium salt. Adv. Colloid Interface Sci. **225**, 16-36 (2015)

[33] A. Bensghaïer, Z. Salmi, B. L. Droumaguet, A. Mekki, A. A. Mohamed, M. Bejia and M. M. Chehimib, Diazonium interface chemistry and click polymerization: A novel route for carbon nanotube-polytriazole nanocomposites. Surf. Interface Anal. **48**, 509-513 (2016)

[34] M. P. Lavin-Lopez, A. Paton-Carrero, L. Sanchez-Silva, J. L. Valverde, A. Romero, Influence of the reduction strategy in the synthesis of reduced graphene oxide. Adv. Powder Technol. **28**, 3195-3203 (2017)

[35] Y. Han and al, Preparation and electrochemical performances of graphene/polypyrrole nanocomposite with anthraquinone-graphene oxide as active oxidant. Carbon. **119**, 111-118, (2017)

[36] Z. Gu and al, Synthesis and characterization of polypyrrole/graphite oxide composite by in situ emulsion polymerization. J. Polym. Sci. Part B Polym. Phys. **48**, 1329-1335 (2010)

[37] R. Bissessur, P. K. Y. Liu, S. F. Scully, Intercalation of polypyrrole into graphite oxide. Synth. Met. **156**, 1023-1027 (2006)

[38] M. S. Dresselhaus, A. Jorio, M. Hofmann, G. Dresselhaus, R. Saito, Perspectives on Carbon Nanotubes and Graphene Raman Spectroscopy. Nano Lett. **10**, 751-758 (2010)

[39] D. Graf and al, Spatially Resolved Raman Spectroscopy of Single- and Few-Layer Graphene. Nano Lett. **7**, 238-242 (2007)

[40] K. N. Kudin, B. Ozbas, H. C. Schniepp, R. K. Prud'homme, I. A. Aksay, R. Car, Raman Spectra of Graphite Oxide and Functionalized Graphene Sheets. Nano Lett. **8**, 36-41 (2008)

[41] J. Zhang, X. S. Zhao, Conducting Polymers Directly Coated on Reduced Graphene Oxide Sheets as High-Performance Supercapacitor Electrodes. J. Phys. Chem. C. **116**, 5420-5426 (2012)

[42] Yongan Niu, Qiuming Zhang, Yao Li, Qinghong Fang, Xin Zhang, "Reduction, dispersity and electrical properties of graphene oxide sheets under low-temperature thermal treatments". J Mater Sci: Mater Electron. **28**, 729–733 (2017)

[43] K. Krishnamoorthy, M. Veerapandian, K. Yun, S.-J. Kim, The chemical and structural analysis of graphene oxide with different degrees of oxidation. Carbon. **53**, 38-49 (2013)

[44] S. Park , Jinho An , Jeffrey R. Potts , Aruna Velamakanni , Shanthi Murali , Rodney S. Ruoff, Hydrazine-reduction of graphite and graphene oxide. Carbon. **49**, 3019 –3023 (2011)

[45] S.T. Navale, A.T. Mane, M.A. Chougule, N. M. Shinde, Highly selective and sensitive CdS thin film sensors for detection of NO_2 gas. RSC Adv. **4**, 44547-44554 (2014)

[46] L. Q. Fan, G. J. Liu, J. H. Wu, L. Liu, J. M. Lin, Y. L. Wei, Asymmetric supercapacitor based on graphene oxide/polypyrrole composite and activated carbon electrodes. Electrochim. Acta. **137**, 26–33 (2014)

[47] M Fang, K Wang, H Lu, Y Yang, S Nutt., Single-layer graphene nanosheets with controlled grafting of polymer chains. J. Mater. Chem. **20**, 1982-1992 (2010)

[48] P. Su, H. Shieh, Flexible NO_2 sensors fabricated by layer-by-layer covalent anchoring and in situ reduction of graphene oxide. Sens. Actuators B **190**, 865–872 (2014)

[49] R. Kumar, S. Singh, A. Misra, Development of NO_2 Gas Sensor Based on Plasma Polymerized Nanostructure Polyaniline Thin Film. J. Miner Mater Char Eng. **9**, 997 (2010)

[50] M. A. Chougule, D. S. Dalavi, S. Mali, P. S. Patil, A. V. Moholkar, G. L. Agawane, J. H. Kim, S. Sen, V.B. Patil, Novel method for fabrication of room temperature polypyrrole–ZnO nanocomposite NO_2 sensor. Measurement. **45**, 1989 (2012)

[51] Tien, H.N. Hur, S.H. One-step synthesis of a highly conductive graphene-polypyrrole nanofiber composite using a redox reaction and its use in gas sensors. Phys. Status Solidi Rapid Res. Lett. **6**, 379–381 (2012)

[52] Y. Yang, S. Li, W. Yang, W. Yuan, J. Xu, Y. Jiang, In Situ Polymerization Deposition of Porous Conducting Polymer on Reduced Graphene Oxide for Gas Sensor. ACS Appl. Mater. Interfaces. **6**, 13807–13814 (2014)

Tables

Table 1 Structural characteristics of Graphitic materials

	D (cm^{-1})	G (cm^{-1})	2D (cm^{-1})	D+D'(cm^{-1})	I_D/I_G
Graphite	1345	1568	2700	/	0,31
GO	1364	1614	2704	2950	1,02
rGO	1350	1574	2658	2919	1,00
rGO-aryl-COOH	1350	1573	2682	2921	1,02

Table 2 Structural characteristics of composites

	D (cm^{-1})	G (cm^{-1})	I_D/I_G
PPy/ GO	1338	1557	1,01
PPy/ rGO	1335	1560	0,89
PPy/ rGO-aryl-COOH	1349	1570	0,84

Table 3 Conductivities of PPy/rGO and PPy/ rGO-aryl-COOH at room temperature

Composites films	Conductivity (s/cm)	Resistivity (Ohm/cm)
PPy/rGO	3.088	$3.238*10^{-1}$
PPy/rGO-aryl-COOH	5.394	$1.854*10^{-1}$

Table 4 Sensor sensitivity variation in function of temperature

Temperature	Sensitivity (%/ppm)
25	1.01
40	0.95
60	0.90
80	0.84

Table 5 Impedance parameters were obtained for PPy/rGO and PPy/ rGO-aryl-COOH sensors by fitting data to the equivalent circuit

	R_c (Ω)	R_1(Ω)	C_1(μF)
Fresh PPy/rGO	4.94	98.35	8.24
NO_2 exposed PPy/rGO	6.79	57.34	15.32
Fresh Ppy/rGO-aryl-COOH	5.78	109.20	6.10
NO_2 exposed PPy/ rGO-aryl-COOH	6.73	61.73	10.80

Table 6 nitrogen dioxide (NO_2) sensor based on nanocomposite polypyrrole and functionalized graphene

Materials	NO_2 concentration	Work temperature	Sensitivity	Response time	Recovery time	Reference
rGO	0.5-20 ppm (air)	RT	-	2500 s	-	[48]
PANI thin film	20 ppm	RT	Ra/Rg	206.19	-	[49]
PPy/ZnO	100 ppm (air)	RT	(Ra-Rg)/Ra=38%	2-4 min	4min	[50]
PPy/rGO	50 ppm (air)	RT	-	-	-	[51]
PEDOT/rGO	0.5 ppm (air)	RT	-	-	-	[52]
PPy/rGO	2 ppm (air)	RT	(Ra-Rg)/Ra=22 %	199 s	145 s	our work
PPy/rGO-aryl-COOH	2 ppm	RT	(Ra-Rg)/Ra=30 %	129 s	114 s	our work

Figures

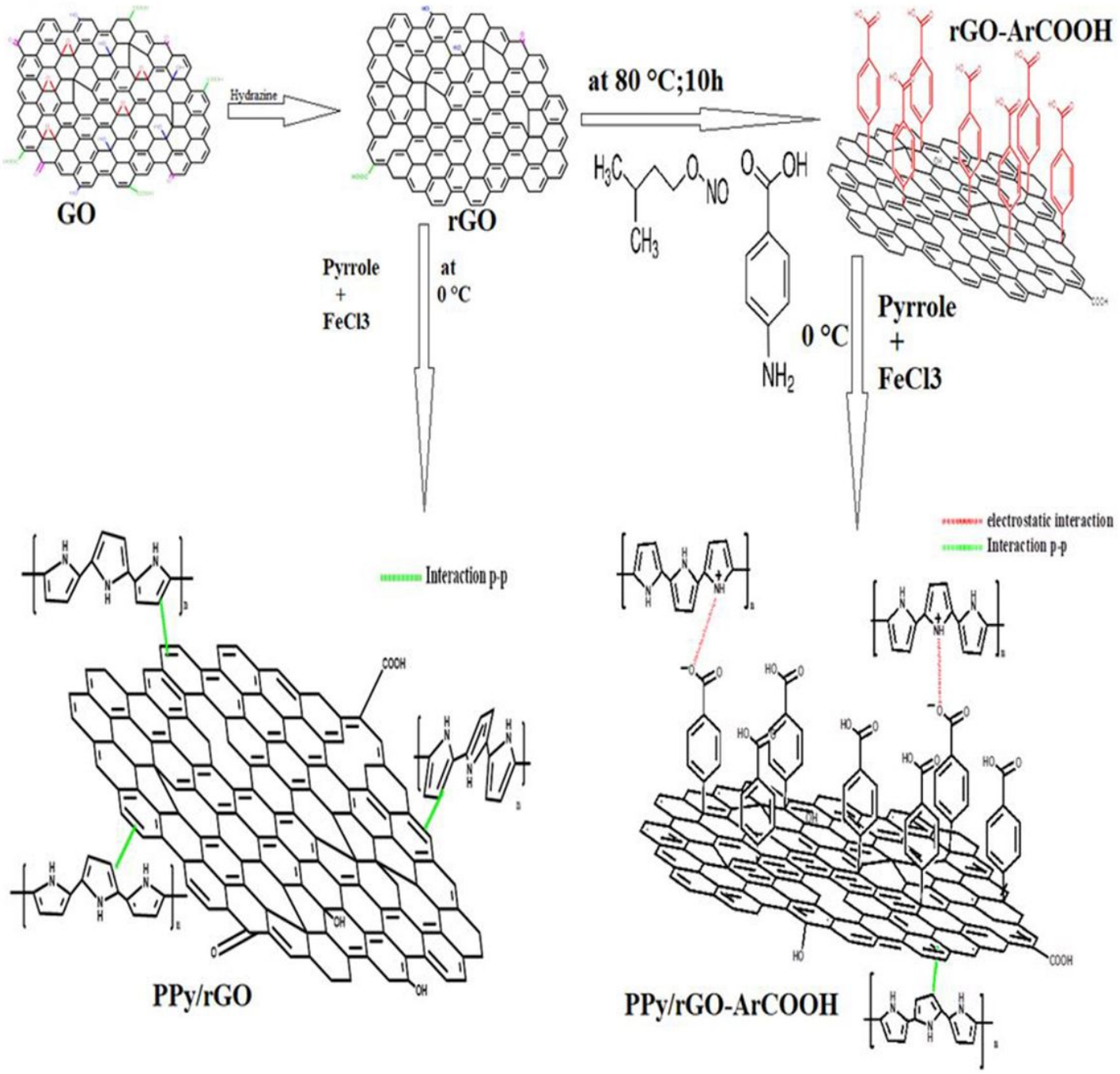

Figure 1

Synthesis steps for growing up polypyrrole on carboxybenzene-functionalized graphene

Figure 2

PPy/ rGO-aryl-COOH deposited on BOPET with spin coating

Figure 3

PPy/rGO deposited on BOPET with spin coating

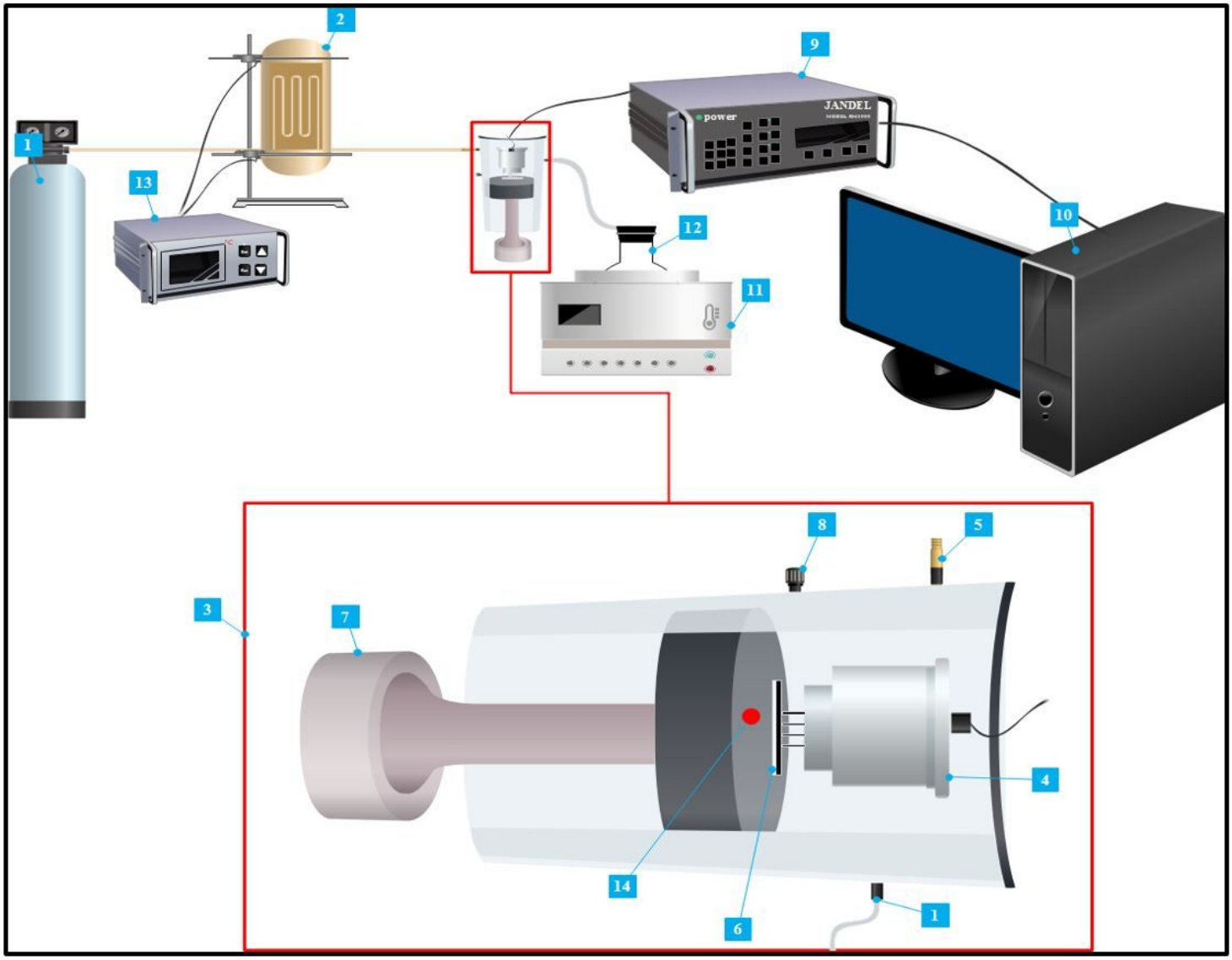

Figure 4

Description of measurement module. 1. Container of nitrogen gas. 2. Heating Element. 3. Test chamber. 4. Measuring head. 5. Cupper canal. 6. Flexible sensitive layer. 7. Piston. 8. Gas vent. 9. Connecting device. 10. Laptop. 11. Heating cap. 12. Boat of water. 13. Temperature controller. 14. Vapor inlet

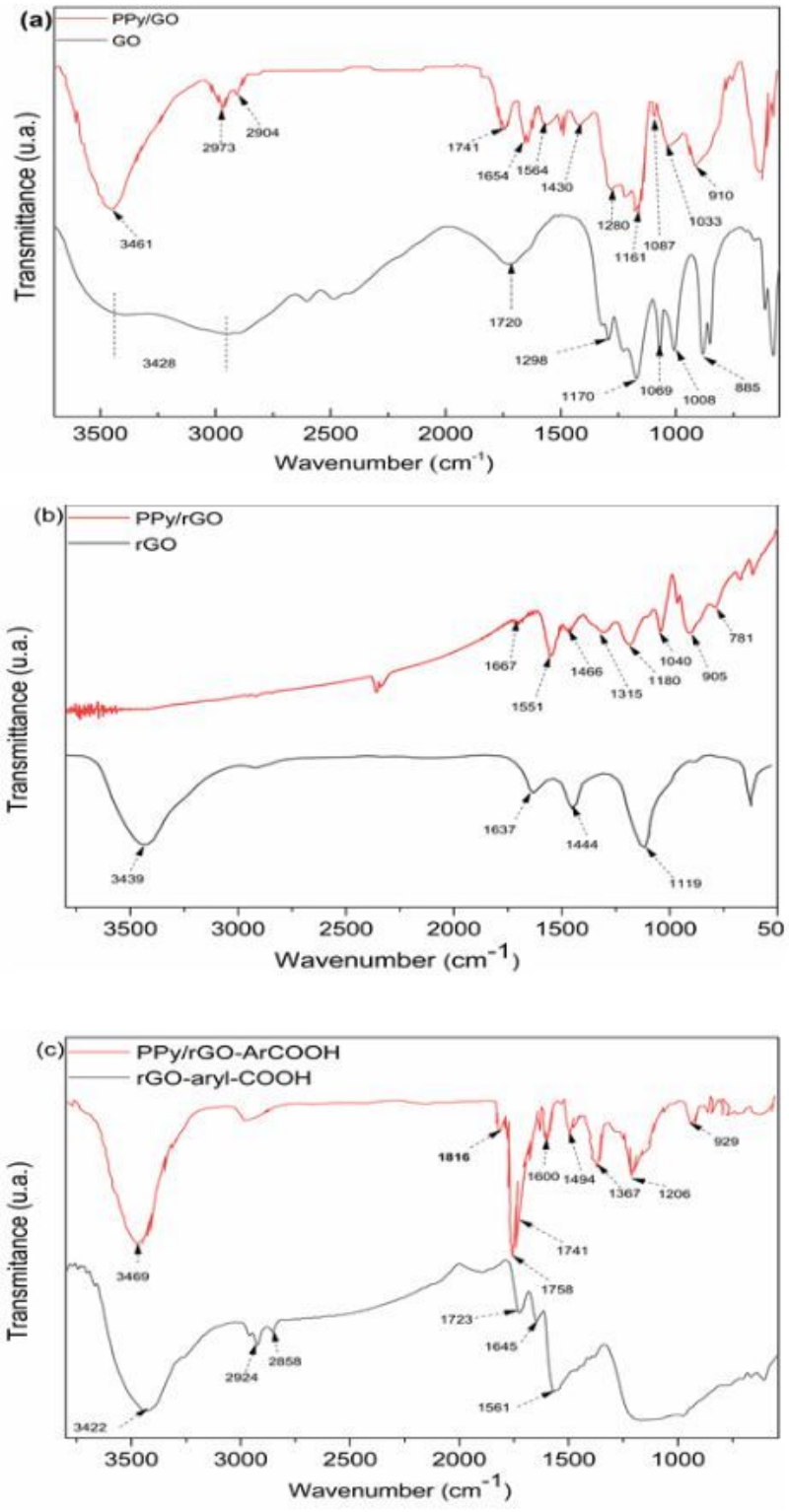

Figure 5

FTIR spectra of graphene and composites

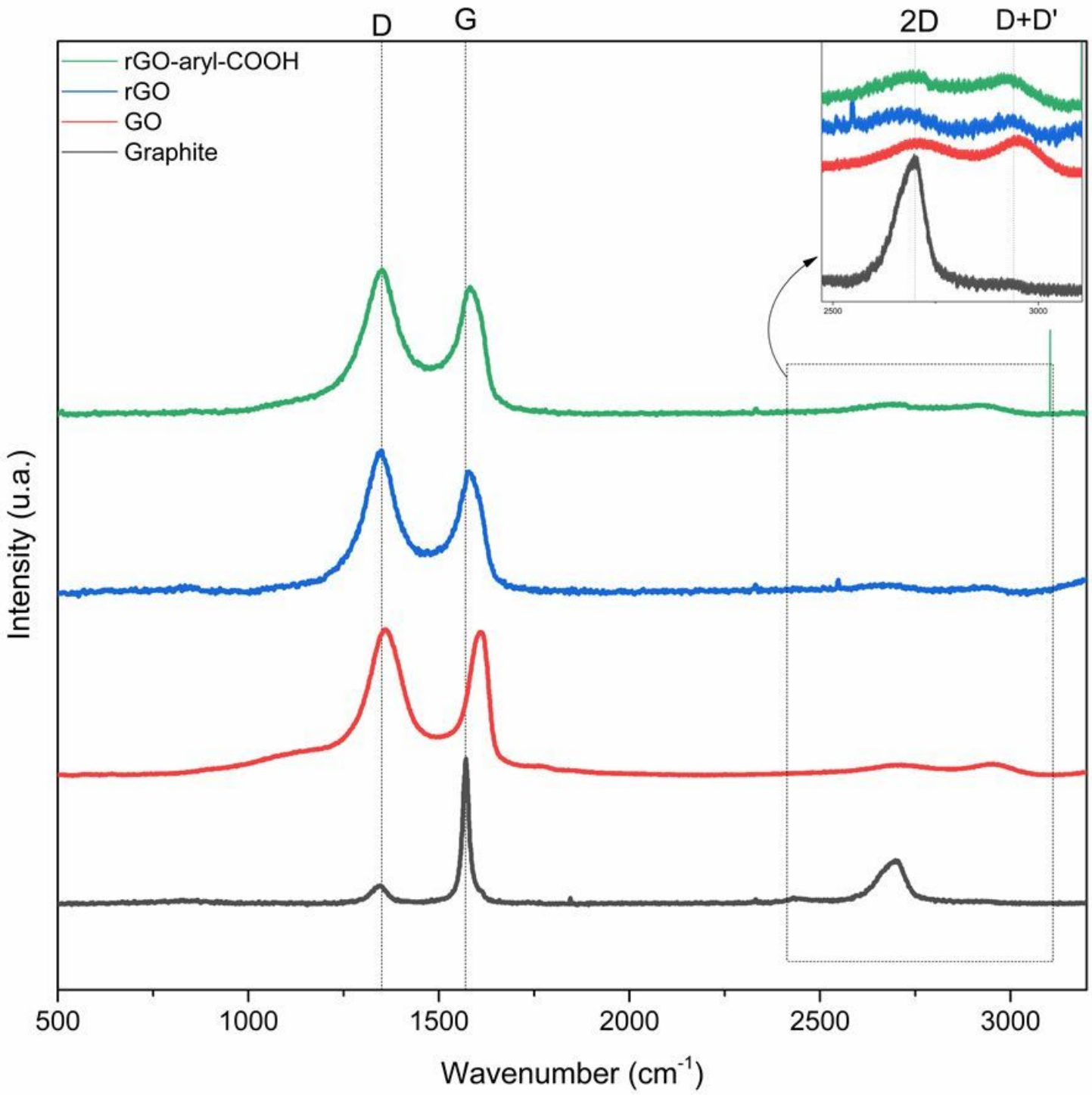

Figure 6

Raman spectra of Graphite, GO, rGO, and rGO-aryl-COOH

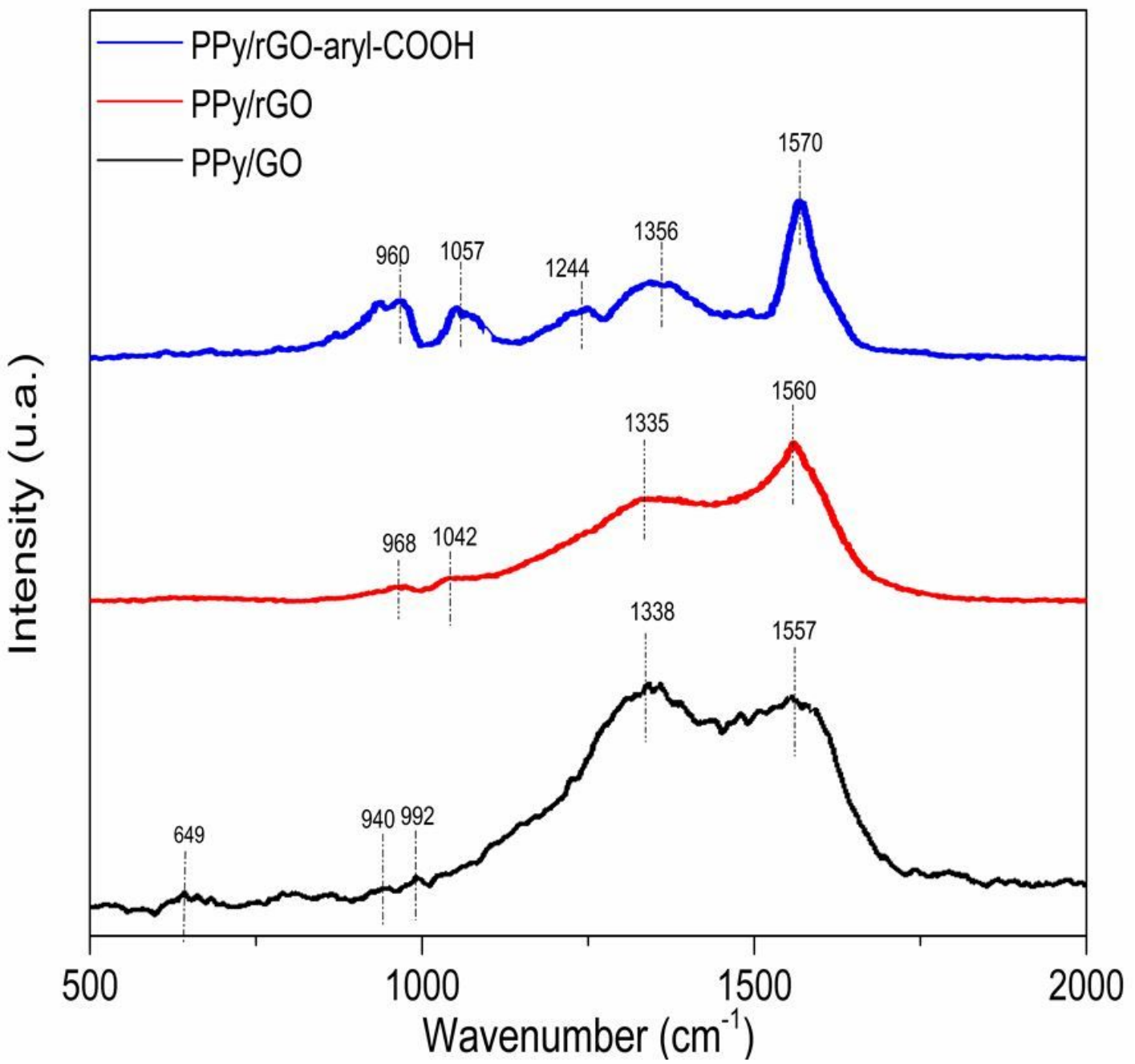

Figure 7

Raman spectra of composites

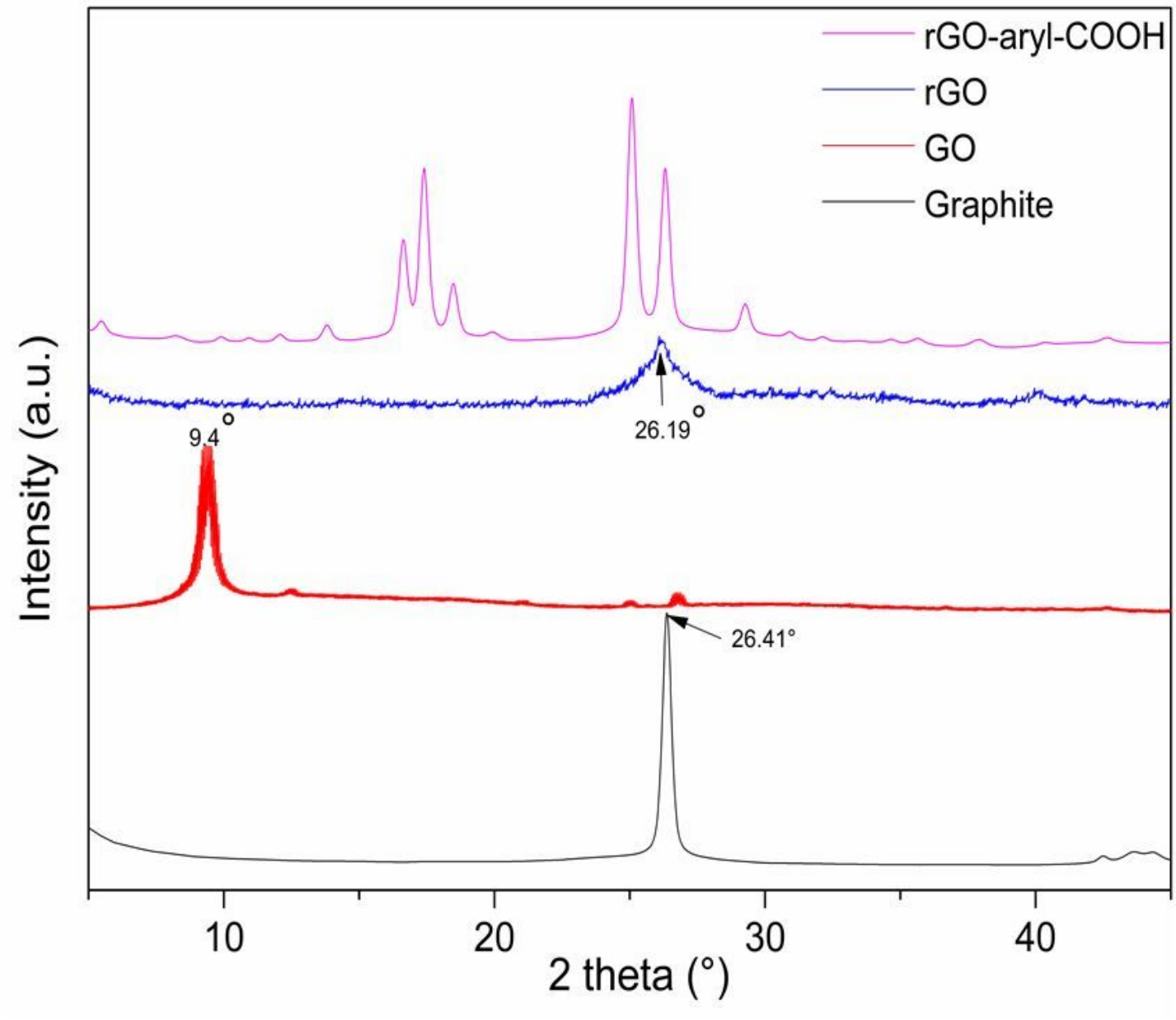

Figure 8

XRD patterns of graphitic materials

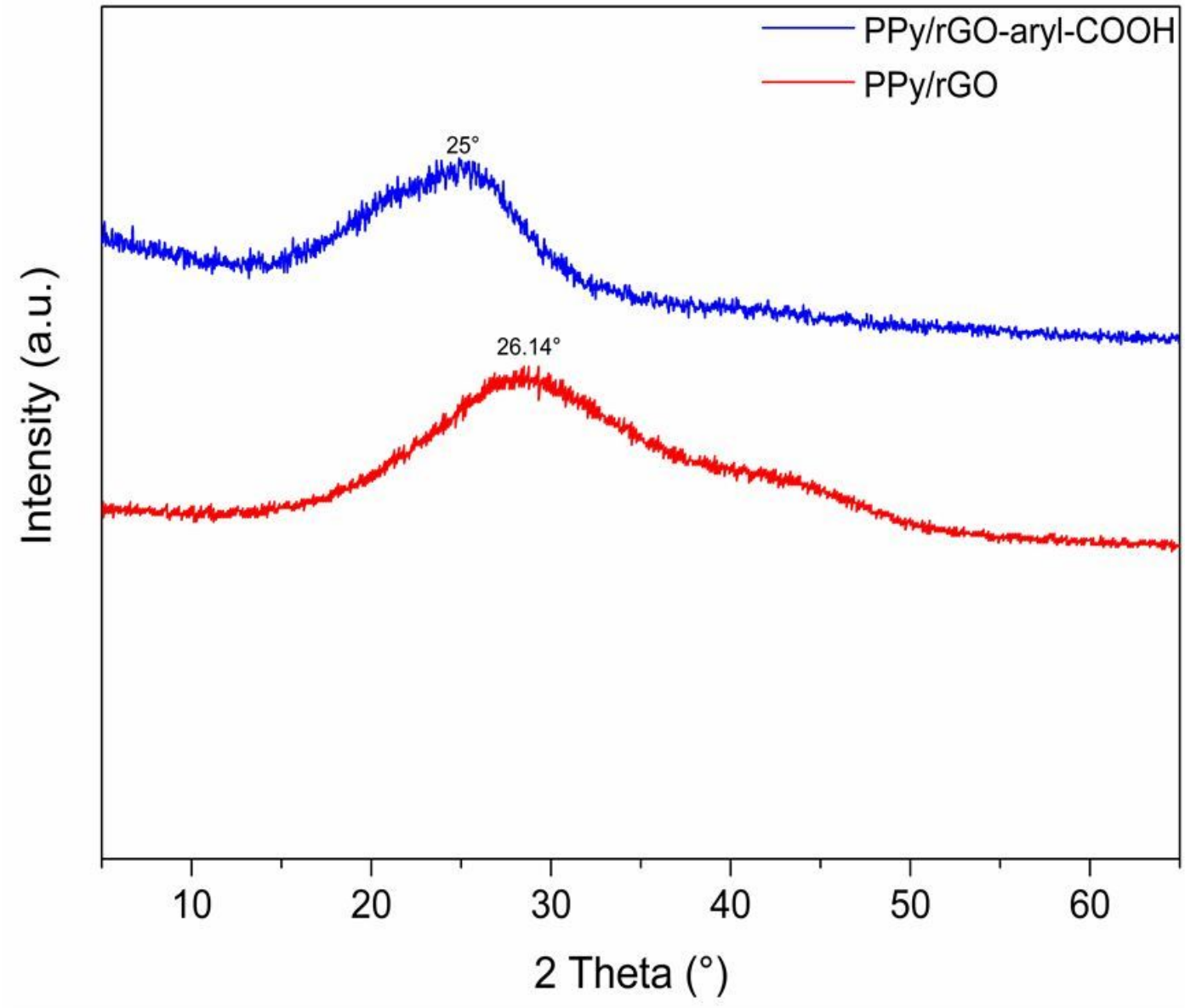

Figure 9

XRD of a PPy/rGO and PPy/ rGO-aryl-COOH nanocomposites

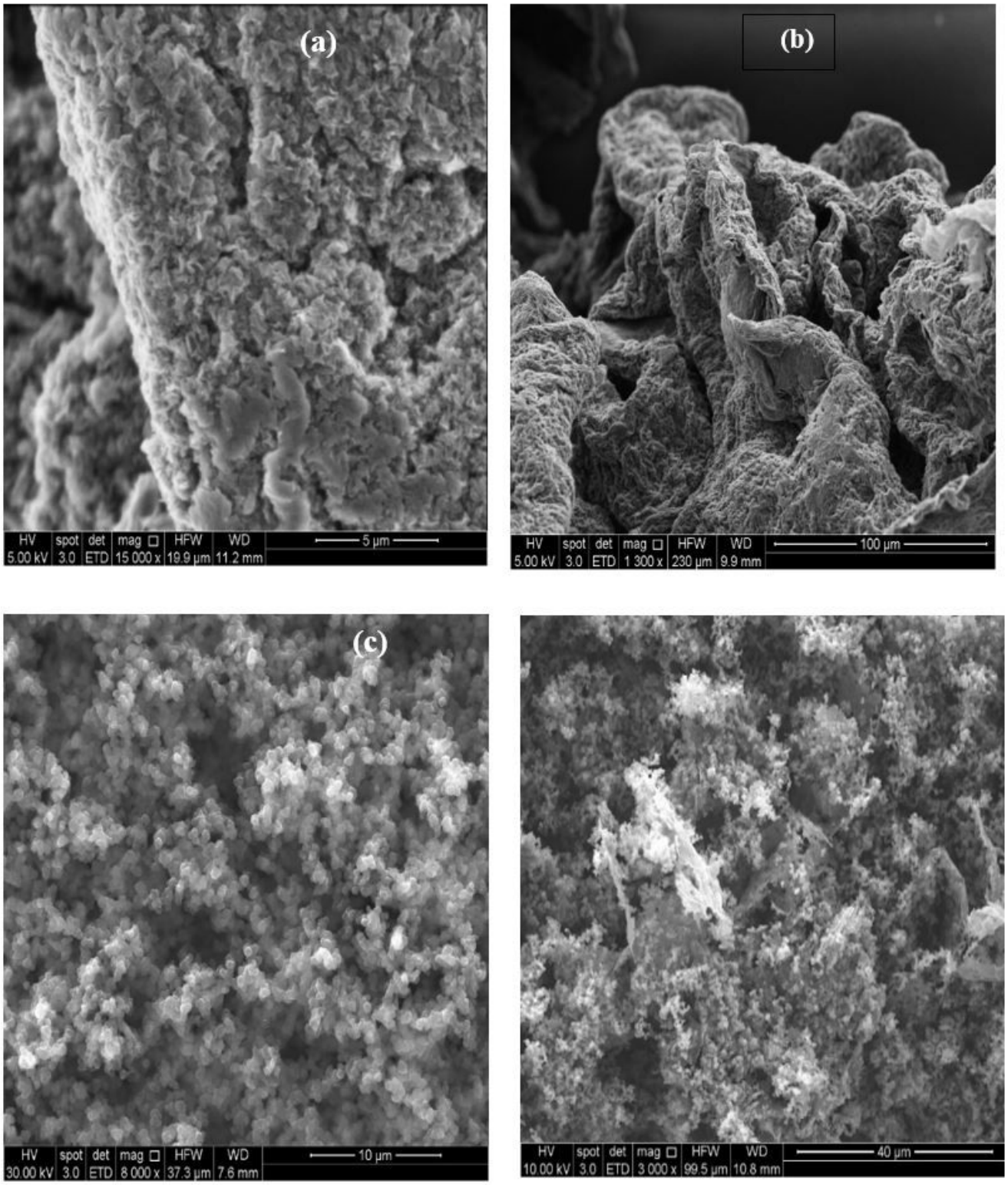

Figure 10

SEM micrographs for (a) rGO, (b) rGO-aryl-COOH, (c) PPy / rGO, (d) PPy / rGO-aryl-COOH

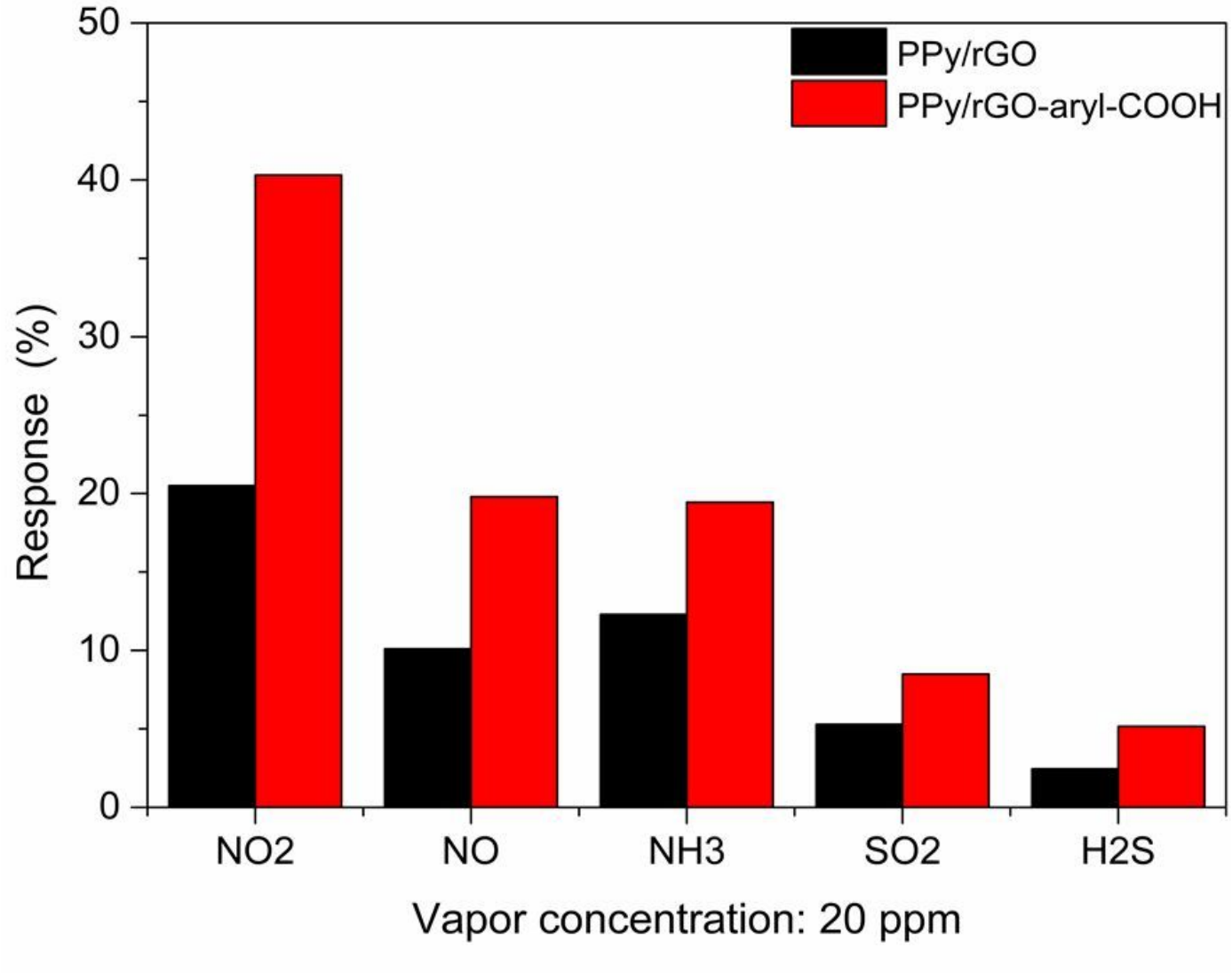

Figure 11

The response of PPy/rGO and PPy/ rGO-aryl-COOH films vis-a-vis gas at a concentration of 20 ppm

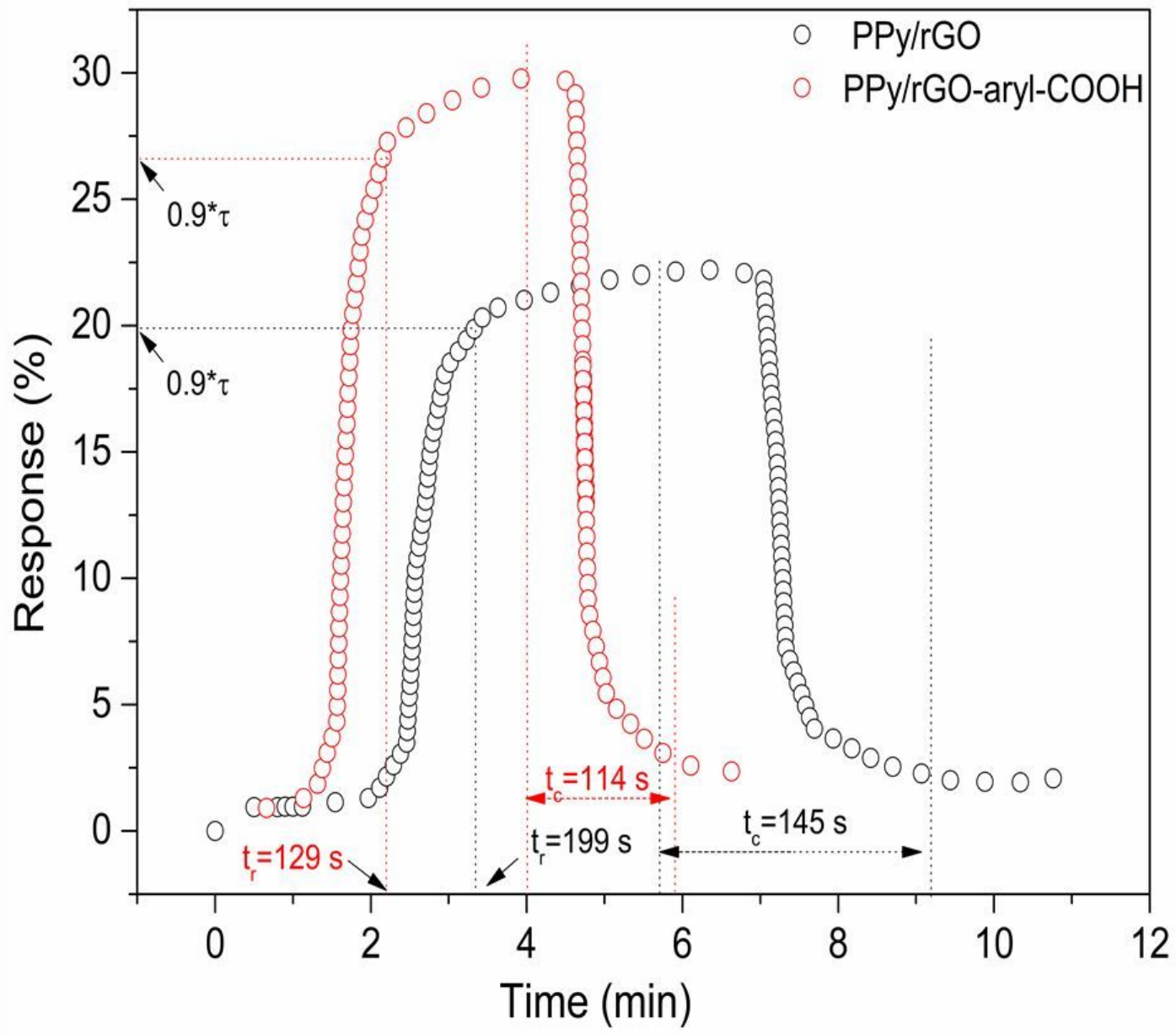

Figure 12

Response rate of 2-ppm NO2 injection on PPy/rGO and PPy/ rGO-aryl-COOH films

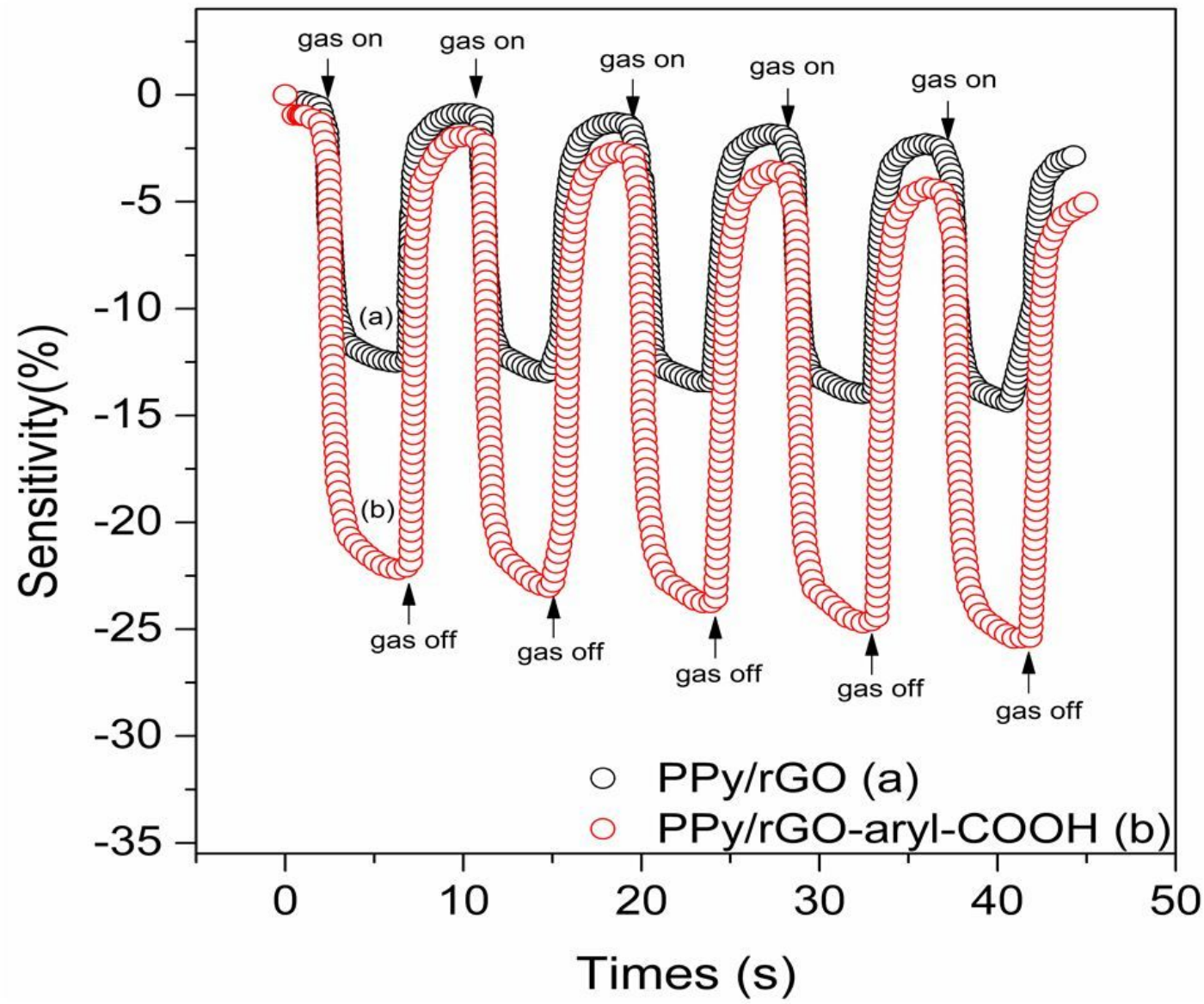

Figure 13

Response reproducibility cycles of nanocomposite toward 2 ppm NO2 (a) PPy/rGO and (b) PPy/rGO-aryl-COOH

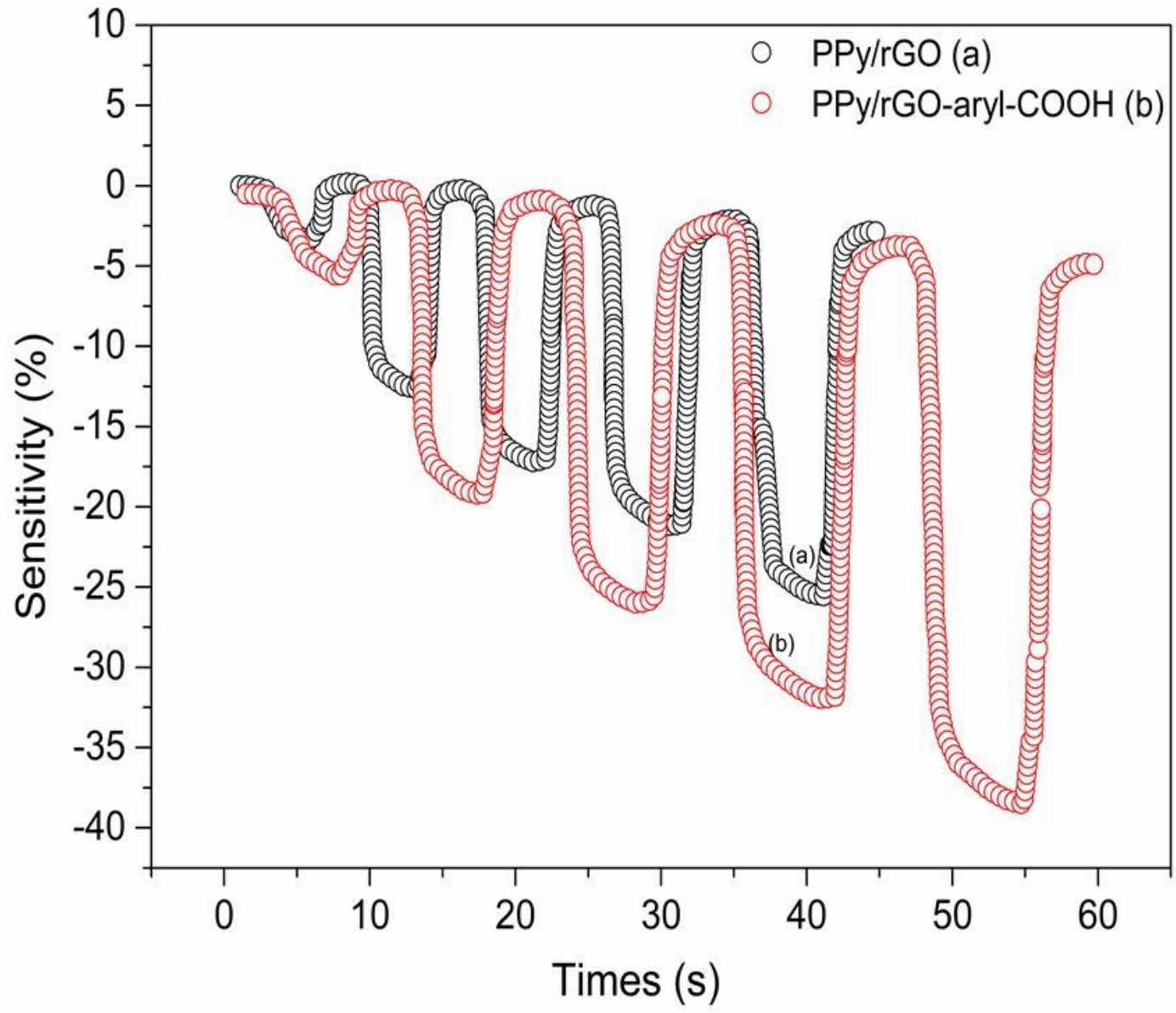

Figure 14

Dynamic response of nanocomposite sensors PPy /rGO (a) and (b) PPy/ rGO-aryl-COOH

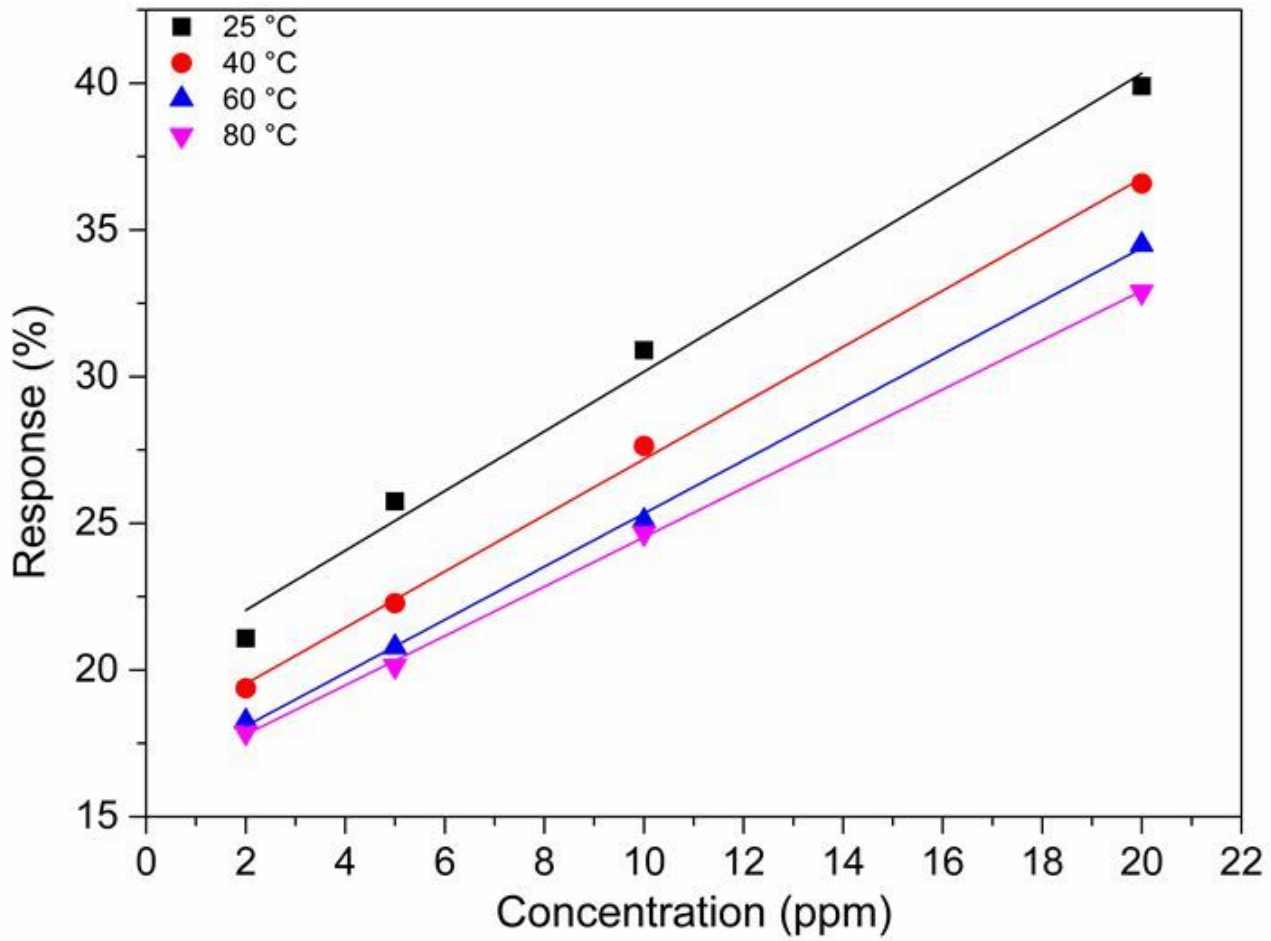

Figure 15

Influence of temperature on the sensor response and sensitivity

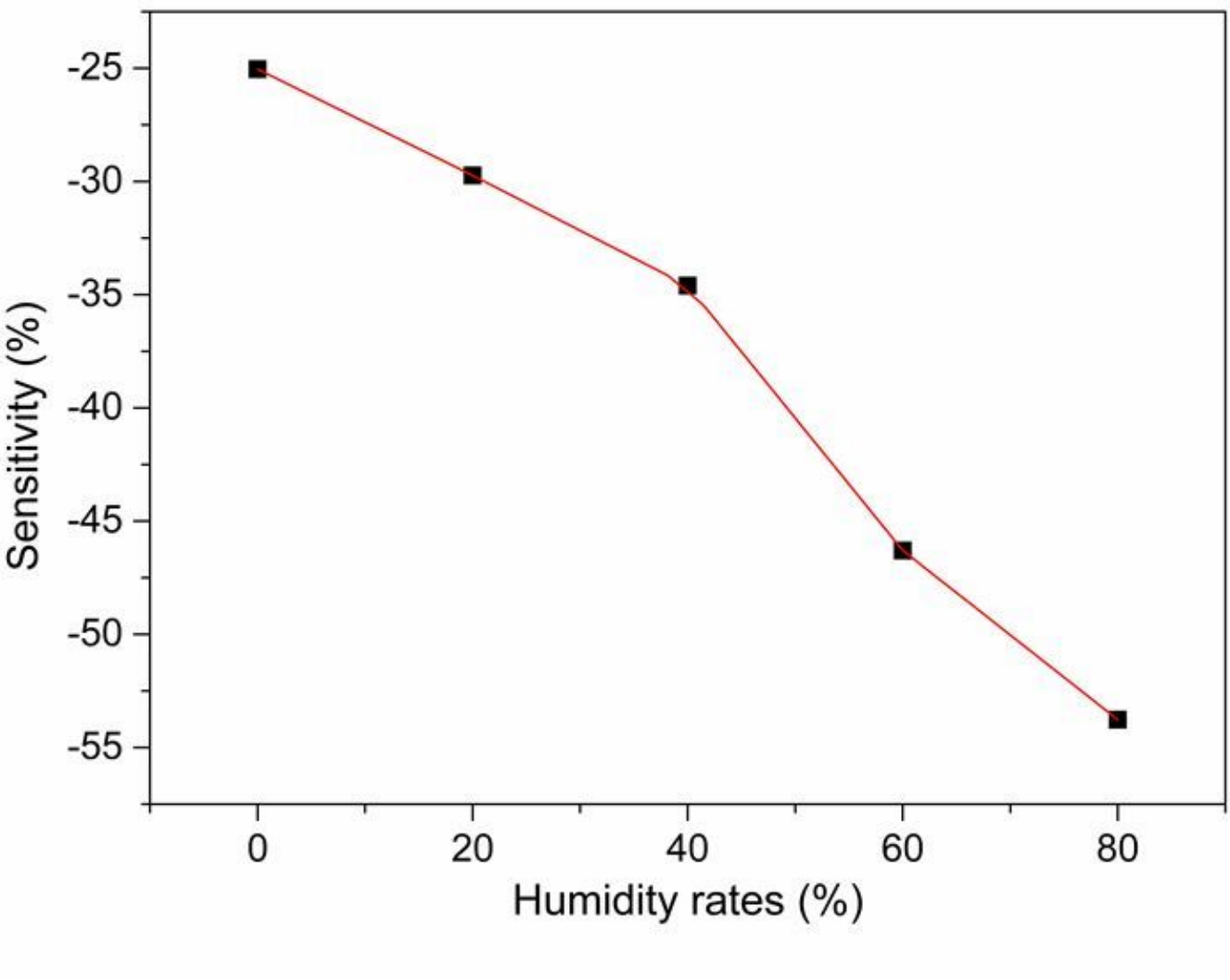

Figure 16

Influence of humidity atmosphere on PPy/ rGO-aryl-COOH responses behavior

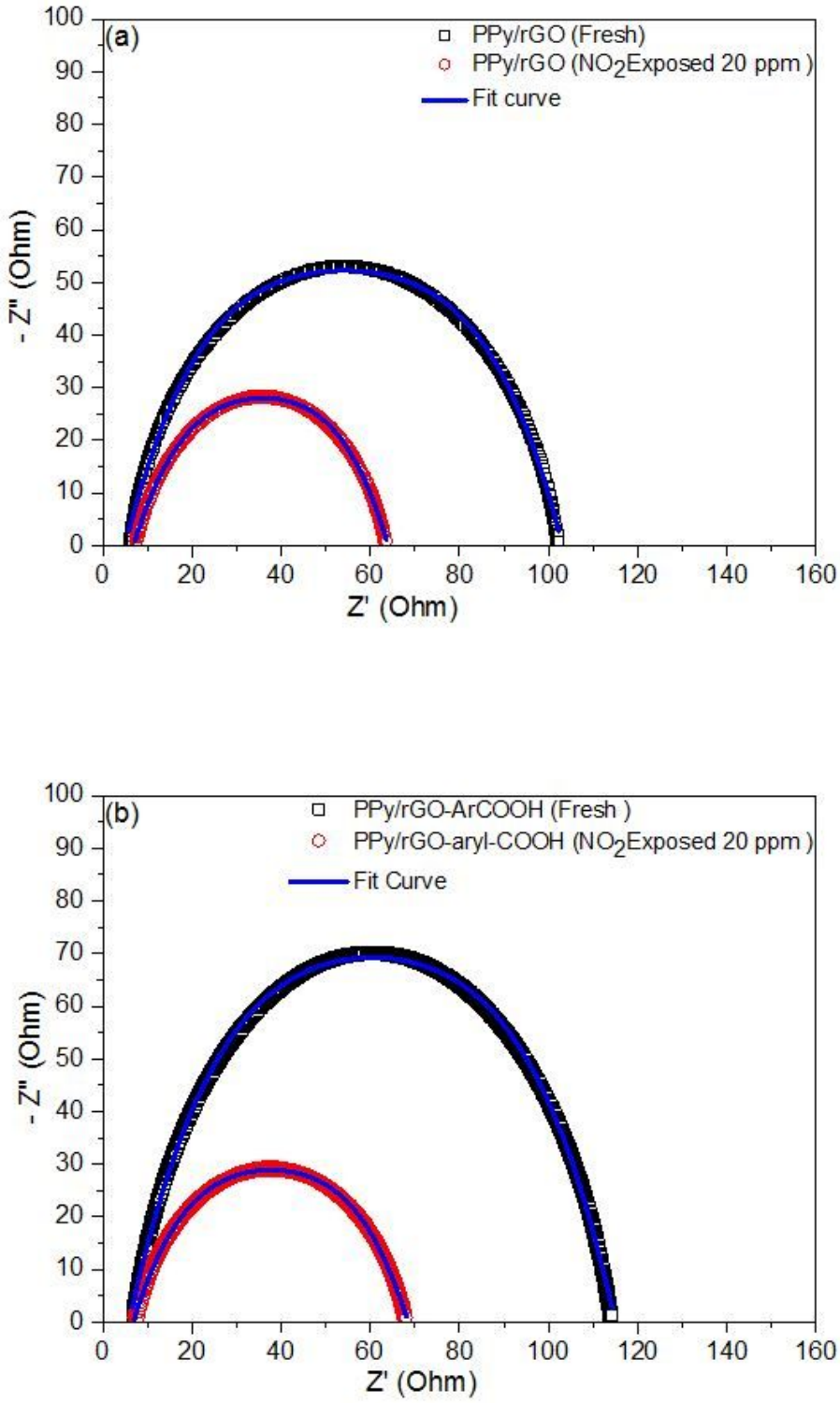

Figure 17

Impedance spectra of PPy/ rGO-aryl-COOH and PPy/rGO under fresh air and NO2 environment

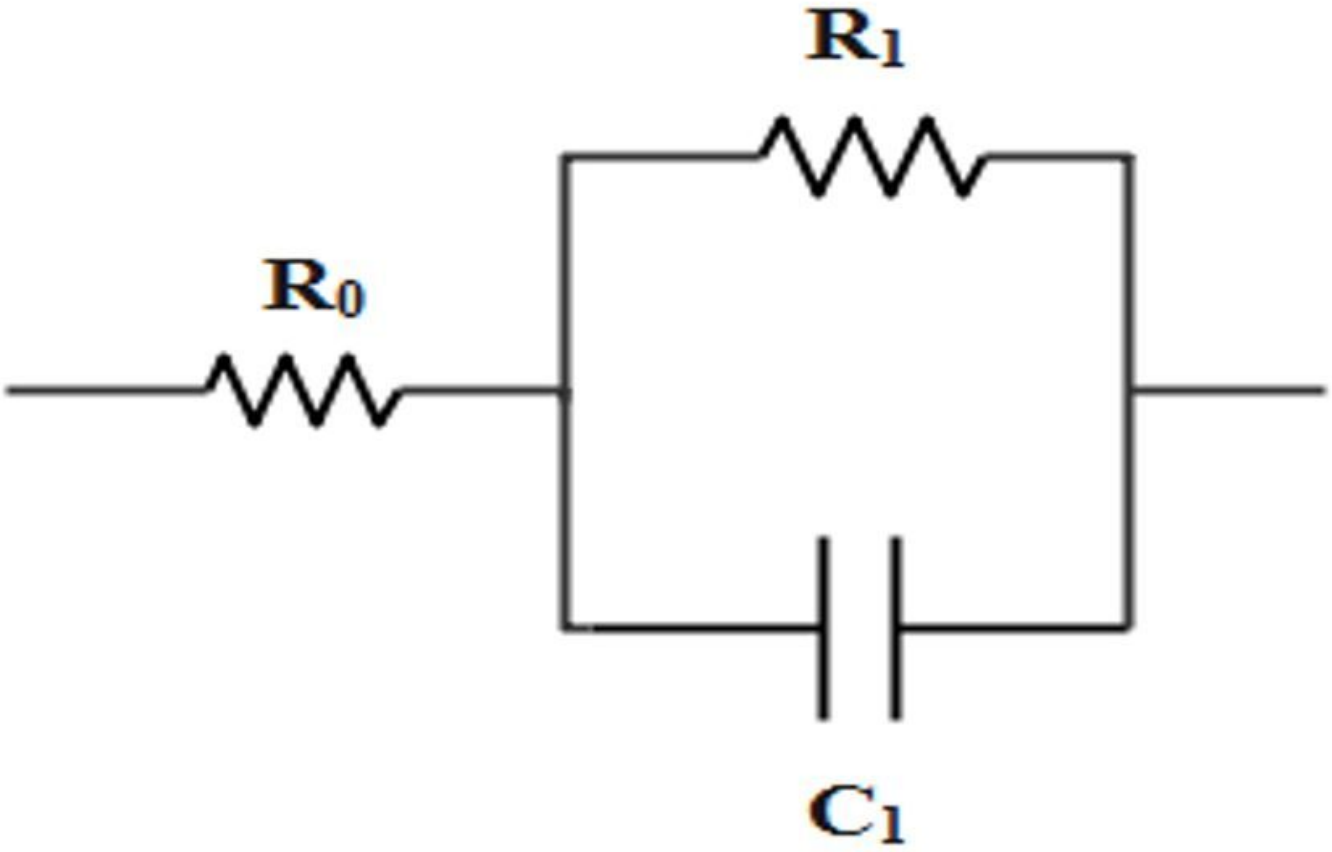

Figure 18

Circuit equivalence